

# Quantum-coherent mixtures of causal relations

Jean-Philippe W. MacLean<sup>1,2,\*</sup>, Katja Ried<sup>1,2,3,\*</sup>, Robert W. Spekkens<sup>3</sup> and Kevin J. Resch<sup>1,2</sup>

<sup>1</sup>*Institute for Quantum Computing, University of Waterloo, Waterloo, Ontario, Canada, N2L 3G1*

<sup>2</sup>*Department of Physics & Astronomy, University of Waterloo, Waterloo, Ontario, Canada, N2L 3G1 and*

<sup>3</sup>*Perimeter Institute for Theoretical Physics,  
Waterloo, Ontario, Canada, N2L 2Y5*

*\*These authors contributed equally to this work.*

Understanding the causal influences that hold among parts of a system is critical both to explaining that system's natural behaviour and to controlling it through targeted interventions. In a quantum world, understanding causal relations is equally important, but the set of possibilities is far richer. The two basic ways in which a pair of time-ordered quantum systems may be causally related are by a cause-effect mechanism or by a common cause acting on both. Here, we show a coherent mixture of these two possibilities. We realize this nonclassical causal relation in a quantum optics experiment and derive a set of criteria for witnessing the coherence based on a quantum version of Berkson's effect, whereby two independent causes can become correlated upon observation of their common effect. The interplay of causality and quantum theory lies at the heart of challenging foundational puzzles, including Bell's theorem and the search for quantum gravity.

## INTRODUCTION

Unraveling the causal mechanisms that explain observed correlations is an important problem in any field that uses statistical data. For example, a positive correlation between the damage done by a fire and the number of fire fighters on scene does not imply that the fire fighters caused the damage. Discovering causal relations has applications ranging from epidemiology and genetics to economics and policy analysis [1, 2]. Causal explanation is also playing an increasingly important role in quantum physics. It has recently gained prominence in the analysis of Bell's theorem and generalizations thereof [3–6]. Furthermore, causal structure is a close proxy for the structure of space-time in general relativity, and it has been suggested that we will have to abandon the notion of definite causal structure and instead allow superpositions thereof in order to develop a theory of quantum gravity [7, 8]. Understanding causality in a quantum world may provide new resources for future quantum technologies as we gain control over increasingly complex quantum systems. For instance, entanglement has been shown to provide a quantum advantage for causal inference in certain causal scenarios [9].

Classically, when two time-ordered variables are found to be statistically correlated, there are different causal mechanisms that could explain this. It could be that the early variable causally influences the later one, or that both are effects of a common cause. Alternatively, the relation could be either cause-effect or common-cause with certain probabilities. Most generally, there may be cause-effect and common-cause mechanisms acting simultaneously. We refer to this as a physical (as opposed to probabilistic) mixture of the two mechanisms.

In a quantum world, there are additional possibil-

ities. Purely common-cause mechanisms are intrinsically quantum if they correspond to entangled bipartite states. Purely cause-effect mechanisms are intrinsically quantum if they correspond to channels that are not entanglement-breaking. But quantum effects are not restricted to only these: as we will show, when common-cause and cause-effect mechanisms act simultaneously, one can have quantum-coherent mixtures of causal relations. While conventional quantum mechanics can describe purely cause-effect and purely common-cause relations, quantum-coherent mixtures can only be represented using recent extensions of the formalism [10?–15], in particular Refs. [9, 16].

Chiribella [17] and Oreshkov *et al.* [14] have investigated coherent combinations of different causal orderings, specifically of  $A$  causing  $B$  and  $B$  causing  $A$ . If realizable, such combinations would constitute a resource for computational tasks [18], with striking applications in gate discrimination [17, 19, 20]. However, this possibility requires that  $A$  and  $B$  are not embeddable into a global causal order, whereas current physical theories implicitly assume such an ordering. By contrast, we study a coherent combination of causal structures wherein  $A$  is always temporally prior to  $B$ , a situation that is compatible with a global ordering and which therefore can be realized experimentally. If the demonstrated applications of superpositions of causal orders noted above can be attributed to the novel possibilities that are allowed by quantum theory for combining causal relations, then other quantum-coherent mixtures of causal relations, such as cause-effect and common-cause, may also constitute a resource.

The present work provides a framework for describing the different ways in which causal relations may be combined and experimental schemes for realizing and

detecting them. We perform an experiment with photonic qubits that implements various such combinations and observes their operational signatures. Our main result is the experimental confirmation of the possibility of preparing a quantum-coherent mixture of common-cause and cause-effect relations.

## RESULTS

### Signatures of different causal mixtures

We seek to classify the causal relations that can hold between two quantum systems and, in particular, to derive and detect an experimental signature of a quantum-coherent mixture of cause-effect and common-cause relations. The tools for this can be illustrated with a simpler example: a mixture of two cause-effect mechanisms in a scenario wherein two distinct causes influence a common effect.

A signature for distinguishing physical from probabilistic mixtures can be derived from Berkson's effect, a phenomenon in classical statistics whereby conditioning on a variable induces statistical correlations between its causal parents when they are otherwise uncorrelated. Figure 1(a,b) provides an intuitive example. Note that the Berkson effect only arises if one has a combination of two causal mechanisms: in Fig. 1, both teaching and research ability influence the hiring decision. Crucially, the strength of the induced correlations can reveal how the two mechanisms are combined. In particular, probabilistic mixtures can only induce relatively weak correlations, as illustrated in Fig. 1(c) and proved rigorously in Supplementary Note 6. Correlations that are stronger than this bound bear witness to a physical mixture of causal mechanisms.

Quantum systems also exhibit the Berkson effect, with the strength of the induced correlations allowing one to distinguish physical from probabilistic mixtures. However, the generalization to quantum systems adds a third category to this classification: post-selection may generate not just classical correlations, but quantum correlations (e.g., entanglement) between the causal parents. We propose that this is a defining feature of a quantum-coherent mixture of causal mechanisms, a full definition of which will be developed below.

### Causal relations between two classical systems

We now turn to the different causal relations between a pair of systems, labelled  $A$  and  $B$ , with  $A$  preceding  $B$  in time. We begin by discussing the case of classical variables, which will motivate our definitions for the quantum

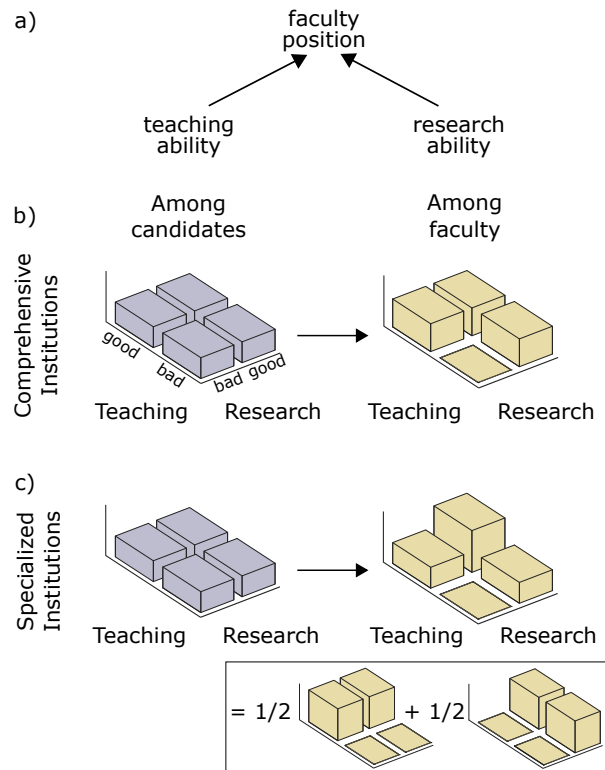


FIG. 1. **An illustration of Berkson's effect when hiring faculty in different institutions.** (a) When applying for faculty positions, a candidate's success generally depends on their skills at both teaching and research. We assume that these abilities are statistically independent in the overall field of applicants. (b) At comprehensive institutions, the hiring process considers both skills and eliminates candidates who are both bad teachers and bad researchers. Consequently, the two abilities become negatively correlated among successful candidates. (c) A set of specialized institutions, each one dedicated either purely to teaching or purely to research, select faculty based solely on the relevant ability in each case - a probabilistic mixture of both causal mechanisms as shown in the inset. Knowing that a candidate was successful in this scenario only reveals information about one of their abilities, and consequently induces weaker negative correlations than in (b), due to the larger fraction of faculty members who are skilled at both.

case. Figure 2(a) depicts the paradigm example, a drug trial, and Fig. 2(b-d) introduces useful representations of the possible causal relations.

Both the example of a randomized drug trial (Fig. 2a, right) and the circuit representation (Fig. 2d, middle) show that a complete description of the causal relation between  $A$  and  $B$  involves two versions of the variable  $A$ : the version prior to the randomizing intervention, denoted  $C$  (treatment preference), has a purely common-cause relation to  $B$ , whereas the post-intervention version,  $D$  (assigned treatment), directly influences  $B$ . The causal relation between  $A$  and  $B$  is therefore completely specified by the stochastic map  $P(CB|D)$ .

This scenario supports a more general version of the Berkson effect: conditioning on recovery can induce cor-

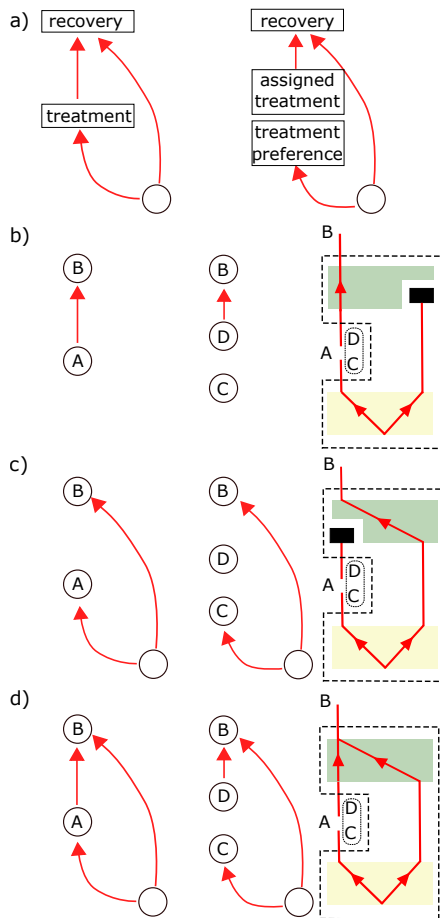


FIG. 2. **Causal relations between two time-ordered systems.** (a) A drug trial aims to discern whether treatment and recovery have a cause-effect relation, whether they share an unobserved common cause, or some combination of both. To this end, pharmaceutical companies randomly assign patients to take either the drug or a placebo, so as to evaluate the cause-effect relation. One may also track treatment preference in order to assess the common-cause relation. A complete characterization of the causal relation requires information about both versions of the treatment variable. Abstract depictions of possible causal relations: (b) purely cause-effect, (c) purely common-cause and (d) general case, including mixtures of both mechanisms. In directed acyclic graphs, arrows represent influences. The variable  $A$  is split into a pre-intervention version, denoted  $C$ , and a post-intervention version, denoted  $D$ . The circuits realizing the causal relations, consisting of a preparation (yellow) of  $A$  and an ancilla, followed by a coupling (green) between  $A$  and the ancilla, which yields  $B$ .

relations not only between the assigned treatment and the unobserved common cause, but also, by extension, between assigned treatment and treatment preference. These correlations bear witness to a combination of common-cause and cause-effect mechanisms, and their strength, as before, can distinguish different classes of combinations.

Before we develop a mathematical representation of these correlations in the quantum case, we first highlight a subtlety of the scenario by appealing to the classical

case. In a randomized drug trial, the assigned treatment is controlled by the experimenter, hence there is no prior distribution over this variable. The object that encodes how assigned treatment correlates with treatment preference in the subpopulation that recovered is therefore not a joint distribution, but a map from assigned treatment to treatment preference. Given the overall stochastic map  $P(CB|D)$ , the subpopulation with  $B = b$  is described by the element  $P(C, B = b|D)$ , which is a subnormalized stochastic map. If one wishes to quantify the correlations encoded in this map using standard measures, one can use the following prescription to construct a joint distribution that is isomorphic to  $P(C, B = b|D)$ : let  $u(D)$  denote the uniform distribution over  $D$  and take  $P^b(CD) \equiv P(C, B = b|D)u(D)/P_b$ , where  $P_b \equiv \sum_{CD} P(C, B = b|D)u(D)$  is a normalization factor. This object encodes the correlations we wish to study in a convenient form and, moreover, admits a close quantum analogue, as we will show.

### Causal relations between two quantum systems

If  $A$  and  $B$  are quantum systems, the input-output functionality of the circuits in Fig. 2 can be characterized using measurements on  $B$  and an analogue of a randomized intervention on  $A$ , that is, a measurement followed by a random reparation. As in the classical case, we split  $A$  into  $C$  and  $D$ . Mathematically, the circuit's functionality is represented by a trace-preserving, completely positive map from states on  $D$  to states on the composite  $CB$ ,  $\mathcal{E}_{CB|D} : \mathcal{L}(\mathcal{H}_D) \rightarrow \mathcal{L}(\mathcal{H}_C \otimes \mathcal{H}_B)$  (where  $\mathcal{L}(\mathcal{H}_X)$  denotes the linear operators over the Hilbert space of  $X$ ), as can be inferred from Refs. [9, 12?–14], and which we term a causal map.

The Berkson effect on quantum systems is formalized as follows: consider a measurement on  $B$ , whose outcomes  $b$  are associated with positive operators  $\{\Pi_B^b\}$ . Finding an outcome  $b$  implies correlations between  $C$  and  $D$ , which are represented by a trace-non-increasing map from  $D$  to  $C$ :  $\mathcal{E}_{C|D}^b \equiv \text{Tr}_B(\Pi_B^b \mathcal{E}_{CB|D})$  (analogous to the subnormalized stochastic map  $P(C, B = b|D)$ ). Equivalently, we can represent this map using the quantum state  $\tau_{CD}^b$  that one obtains by taking the operator that is Choi-isomorphic [21] to  $\mathcal{E}_{C|D}^b$  and normalizing it to have unit trace (analogous to the normalized distribution  $P^b(CD)$ ). The correlations between  $C$  and  $D$  embodied in the map  $\mathcal{E}_{C|D}^b$  can then be assessed using standard measures of correlation on the state  $\tau_{CD}^b$ . We say that the causal map exhibits a Quantum Berkson Effect if there exists a measurement  $\{\Pi_B^b\}$  such that for every outcome  $b$ , the induced correlations between  $C$  and  $D$ , described by  $\tau_{CD}^b$ , are quantum. For the purposes of this article, we take the presence of entanglement as a sufficient condition for quantumness. Thus, our condition is

that each  $\tau_{CD}^b$  be entangled, or equivalently, that each  $\mathcal{E}_{C|D}^b$  be non-entanglement-breaking. Using these definitions, we will now propose a classification of the possible causal relations between two quantum systems, as well as ways of distinguishing the classes.

A causal map  $\mathcal{E}_{CB|D}$  is purely cause-effect if it has the form  $\mathcal{E}_{CB|D}(\cdot) = \mathcal{E}_{B|D}(\cdot) \otimes \rho_C$  (the analogue of  $P(CB|D) = P(B|D)P(C)$ ), which makes it compatible with the causal structure in Fig. 2(b); and purely common-cause if  $\mathcal{E}_{CB|D}(\cdot) = \rho_{CB} \text{Tr}_D(\cdot)$  (the analogue of  $P(CB|D) = P(CB)$ ), which makes it compatible with the causal structure in Fig. 2(c). A causal map is said to be a probabilistic mixture of cause-effect and common-cause relations if there is a hidden classical control variable,  $J$ , which influences only  $B$ , such that for every value of  $J$ , either  $B$  depends only on  $D$  or  $B$  depends only on its common cause with  $C$ . We show in Supplementary Note 1 that every such causal map can be expressed as having just one term of each type,  $\mathcal{E}_{CB|D} = w\mathcal{E}_{B|D} \otimes \rho_C + (1-w)\rho_{CB} \otimes \text{Tr}_D$ , where  $0 \leq w \leq 1$  and  $\text{Tr}_B \rho_{CB} = \rho_C$ . The fact that the marginal on  $C$  is the same in both terms follows from demanding that the control variable  $J$  does not influence  $C$ . This demand is justified by noting that a probabilistic mixture of causal maps that are all purely cause-effect should also be purely cause-effect, but if the switch variable  $J$  implementing this mixture could influence  $C$  in addition to  $B$ , then it would itself constitute a common cause of  $A$  and  $B$ . If a causal map is not such a probabilistic mixture, then it is termed a physical mixture of cause-effect and common-cause mechanisms.

Another distinction that is important for classifying causal relations between two quantum systems is whether the common-cause or cause-effect pathways of a given causal map are themselves quantum or not. We propose that a sufficient condition for quantumness of the common-cause pathway is that there exists an orthogonal basis of states on  $D$ , indexed by  $d$  and denoted  $\rho_d$ , such that the states on  $CB$  induced by these preparations,  $\tau_{CB}^d \equiv \mathcal{E}_{CB|D}(\rho_d)$ , are entangled. Similarly, a causal map is intrinsically quantum on the cause-effect pathway if there exists a measurement on  $C$  that distinguishes a complete set of orthogonal states, indexed by  $c$  and represented by projectors  $\Pi_C^c$ , such that the induced correlations between  $D$  and  $B$  are quantum for every outcome  $c$ . By the same reasoning established in the discussion of the Quantum Berkson Effect, these correlations are represented by trace-non-increasing maps from  $D$  to  $B$ ,  $\mathcal{E}_{B|D}^c \equiv \text{Tr}_C(\Pi_C^c \mathcal{E}_{CB|D})$ , or equivalently by the normalized Choi-isomorphic states  $\tau_{BD}^c$ . This allows us to propose a sufficient condition for quantumness in the cause-effect pathway that closely resembles the one for the common-cause pathway: the states  $\tau_{BD}^c$  must be entangled for all  $c$ .

These distinctions give rise to eight classes of causal

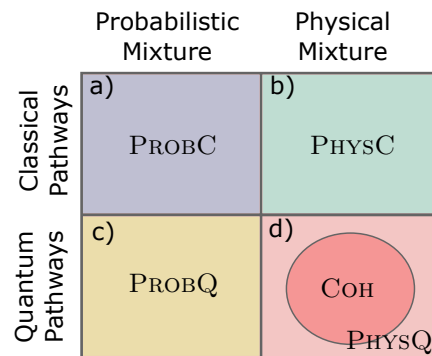


FIG. 3. **Classification of mixtures of causal relations between two quantum systems.** One can distinguish whether the common-cause and cause-effect pathways are effectively classical or whether they are quantum, and whether they are combined in a probabilistic or a physical mixture. This gives rise to four categories of interest: a probabilistic mixture that is classical on both pathways (PROBC), a physical mixture that is classical on both pathways (PHYSC), a probabilistic mixture that is quantum on both pathways (PROBQ), and a physical mixture that is quantum on both pathways (PHYSQ). We leave aside cases wherein only one pathway is quantum. The focus of this paper is the class COH, which exhibits the Quantum Berkson Effect and therefore describes quantum-coherent mixtures of common-cause and cause-effect relations between  $A$  and  $B$ .

maps. We here limit our attention to cases where the pathways are either both quantum or both classical, yielding four classes of interest, illustrated in Fig. 3 and termed PROBC, PHYSC, PROBQ and PHYSQ. The definition of the fifth class (COH) is the central theoretical proposal of this article: a mixture of common-cause and cause-effect relations is quantum-coherent if the causal map is intrinsically quantum in both the common-cause and cause-effect pathways and it exhibits a Quantum Berkson Effect. We note that the second requirement can only be satisfied if the causal map is a physical mixture, while the first implies that it is quantum in both pathways, hence COH is contained in PHYSQ. We show in Supplementary Note 2 that the inclusion is in fact strict.

### Realizing COH with a quantum circuit

Figure 4 presents quantum circuits that realize causal relations between two qubits exemplifying each of the classes. Here,  $E$  denotes the system that mediates between  $B$  and its common cause with  $C$ . System  $F$  is introduced to make the gate  $\mathcal{E}_{BF|DE}$  preserve dimensionality, but it is discarded afterwards. The initial state  $\rho_{CE}$  in all cases is the maximally entangled state

$$|\Phi^+\rangle \equiv \frac{1}{\sqrt{2}}(|HH\rangle + |VV\rangle), \quad (1)$$

where  $|H\rangle, |V\rangle$  denote the eigenstates of the Pauli operator  $\sigma_z$ , anticipating the identification as horizontal and vertical polarization states of our photonic qubits. The gate  $\mathcal{E}_{BF|DE}$  that realizes a coherent mixture applies the partial swap unitary,

$$U_{BF|DE} = \frac{1}{\sqrt{2}} \mathbb{1}_{B|D} \otimes \mathbb{1}_{F|E} + i \frac{1}{\sqrt{2}} \mathbb{1}_{B|E} \otimes \mathbb{1}_{F|D}, \quad (2)$$

where  $\mathbb{1}_{Y|X}$  denotes the identity operator from  $X$  to  $Y$ . This unitary coherently combines the two-qubit identity operator,  $\mathbb{1}_{B|D} \otimes \mathbb{1}_{F|E}$ , which realizes a purely cause-effect relation between  $A$  and  $B$ , and the swap operator,  $\mathbb{1}_{B|E} \otimes \mathbb{1}_{F|D}$ , which realizes a purely common-cause relation.

Combining the circuit elements  $\rho_{CE}$  and  $\mathcal{E}_{BF|DE}$  and tracing out  $F$ , we find

$$\begin{aligned} \mathcal{E}_{CB|D}(\cdot) = & \frac{1}{2} \left[ \frac{1}{2} \mathbb{1}_C \otimes \mathcal{I}_{B|D}(\cdot) \right] + \frac{1}{2} |\Phi^+\rangle \langle \Phi^+|_{CB} \text{Tr}_D(\cdot) \\ & - i \left\{ \left[ \frac{1}{2} \mathbb{1}_C \otimes \mathcal{I}_{B|D}(\cdot) \right] |\Phi^+\rangle \langle \Phi^+|_{CB} \right. \\ & \left. - |\Phi^+\rangle \langle \Phi^+|_{CB} \left[ \frac{1}{2} \mathbb{1}_C \otimes \mathcal{I}_{B|D}(\cdot) \right] \right\}. \end{aligned}$$

The first term applies the identity channel from  $D$  to  $B$ ,  $\mathcal{I}_{B|D}$ , whereas the second prepares  $C$  and  $B$  in the maximally entangled state  $|\Phi^+\rangle$ . The cross terms encode coherences between these two causal relations. One can verify that this causal map is quantum in both the cause-effect and the common-cause pathway. It also exhibits a Quantum Berkson Effect: if  $B$  is measured to be in the state  $|H\rangle$ , then

$$\tau_{CD}^H = \frac{1}{2} |HH\rangle \langle HH| + \frac{1}{2} |\varphi\rangle \langle \varphi| \quad (3)$$

where  $|\varphi\rangle \equiv \frac{1}{\sqrt{2}}(|HV\rangle - i|VH\rangle)$ , hence  $\tau_{CD}^H$  is entangled. If instead  $B$  is measured to be in the state  $|V\rangle$ ,  $\tau_{CD}^V$  is similarly entangled. The causal map therefore belongs to COH.

The example of PROBQ from Fig. 4(c) obtained by replacing the partial swap with an equal probabilistic mixture of identity and swap, which eliminates the cross terms in equation (3). The result is a manifestly probabilistic mixture of causal relations that is nevertheless quantum on both pathways. One can further modify this gate to realize the example of PROBC in Fig. 4(a) complete dephasing operations on its inputs,  $D$  and  $E$ , which effectively reduces both qubits to classical bits.

The example of PHYSC presented in Fig. 4(b) also begins by complete dephasing on  $D$  and  $E$  to ensure that both pathways are indeed classical. The simplest example of a physical mixture would then be one wherein  $B$  is a nontrivial function of both  $D$  and  $E$ . However, since we wish to realize all of these examples with a single experimental set-up, we consider instead a probabilistic

mixture of two gates, one of which has  $B$  as a nontrivial function of both  $D$  and  $E$ , whereas the other prepares  $B$  in the completely mixed state. The expression  $\mathcal{E}_{CB|D}$  for each example and the proof that they are all indeed representatives of their classes are provided in the Supplementary Note 2.

### Experimental signatures of causal relations

The four circuits of Fig. 4 are experimentally realized using the set-up of Fig. 5. The polarization degrees of freedom of different photon modes constitute the qubits in our circuit. We use downconversion to prepare the photonic modes  $C$  and  $E$  in the maximally entangled polarization state  $|\Phi^+\rangle$ .

To realize our example of COH (Fig. 4(d)), the partial swap in equation (2) is implemented using linear optics [22]. Here, we significantly improve the stability of the experimental concept of Ref. [22] by incorporating the working principle around a displaced Sagnac interferometer. The other three examples from Fig. 4 are obtained by variations on this set-up. Delaying the photon in mode  $E$  relative to the one in mode  $D$  prevents two-photon interference at the first beam splitter of the Sagnac interferometer, so that the interferometer implements a probabilistic mixture of identity and swap operations (our example of PROBQ, Fig. 4(c)). This latter circuit realizes the same causal map implemented in Ref. 3, which focused on the task of resolving probabilistic mixtures of cause-effect and common-cause relations. However, the experimental setup of Ref. 3 could not realize physical mixtures, which are required to address the broader question, investigated in the present work, of how these two extremes may be combined in general.

Both causal pathways can be made classical by passing the modes through completely dephasing channels on  $D$ ,  $E$  and  $B$ . The example of PROBC from Fig. 4(a) is realized by dephasing in the  $\{|H\rangle, |V\rangle\}$  basis on all three. The example of PHYSC from Fig. 4(b) is also achieved by implementing complete dephasing, but in different bases:  $\{|R\rangle, |L\rangle\}$  on  $D$ ,  $\{|D\rangle, |A\rangle\}$  on  $E$  and  $\{|H\rangle, |V\rangle\}$  on  $B$ . For further details on how to implement the four example classes of causal structures using a single experimental setup, see Supplementary Note 3.

We characterize the causal maps realized in the experiment using tomography [9, 12? ?]: measurements on  $C$  and  $B$  and preparations on  $D$ , each ranging over the six eigenstates of Pauli observables, allow us to reconstruct the map using a least-squares fit. The causal maps obtained from the four circuits in Fig. 4 are shown in Fig. 6 and achieve fidelities above 93% with their respective targets. Although these maps encode a complete description of the causal relation realized between  $A$  and  $B$ , since our goal is only to classify the causal relation,

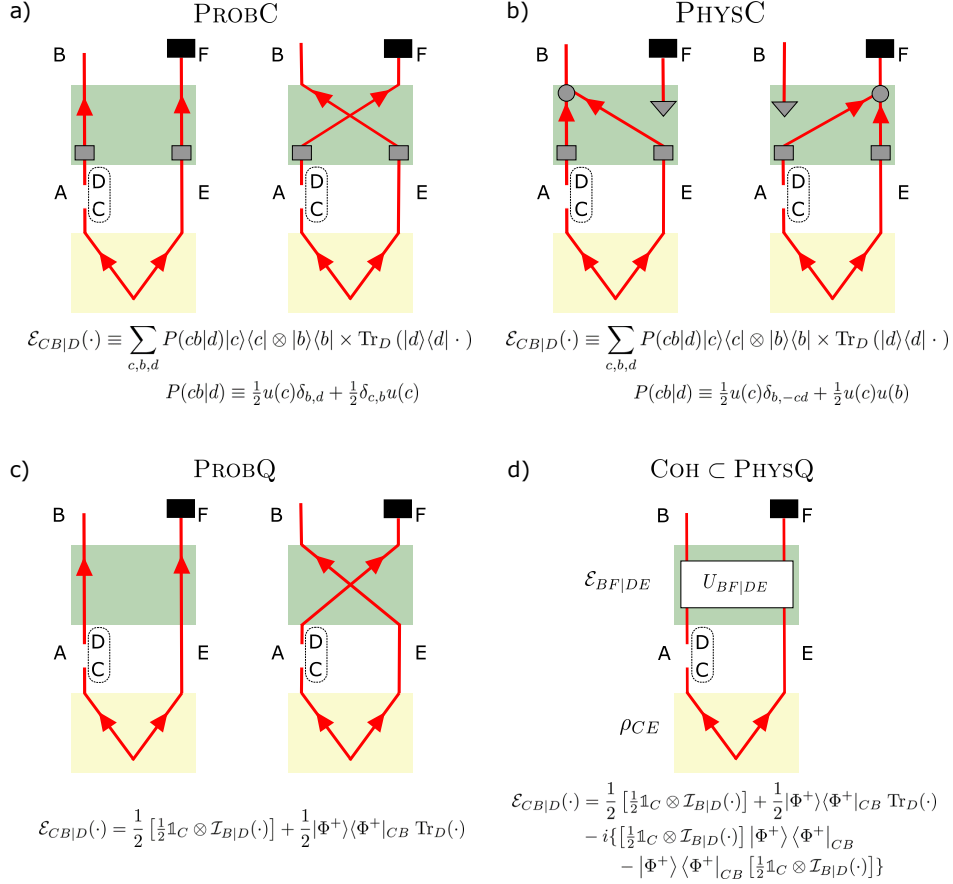


FIG. 4. **Quantum circuits which realize examples of different classes of causal relations between two qubits.** Circuits for four combinations of cause-effect and common-cause mechanisms: **a)** PROBC, **b)** PHYSC, **c)** PROBQ, **d)** COHC PHYSQ. In all circuits,  $C$  and  $E$  are initially prepared in the maximally entangled state  $|\Phi^+\rangle$  and  $F$  is discarded at the end. The examples differ only in the choice of the gate  $\mathcal{E}_{BF|DE}$ , as described in the text. Panels with two circuits represent an equal probabilistic mixture of both scenarios. Black squares represent the trace operation, grey squares represent complete dephasing operations, grey triangles represent preparations of the completely mixed state, grey circles represent the classical XNOR gate, which sets  $b = -ed$  for binary variables  $b, e, d$  taking the values  $\{\pm 1\}$ , and the two-qubit unitary  $U_{BF|DE}$  is the partial swap given by equation (2). Below each example, we specify the causal map  $\mathcal{E}_{CB|D}$  obtained from the state  $\rho_{CE}$  and the gate  $\mathcal{E}_{BF|DE}$  via  $\mathcal{E}_{CB|D}(\cdot) = \text{Tr}_F \circ \mathcal{E}_{BF|DE}(\cdot \otimes \rho_{CE})$ . Lowercase letters  $c, b, d$  represent classical binary variables,  $P(cb|d)$  represents a conditional probability distribution over these,  $\delta_{x,y}$  denotes the Kronecker delta function, and  $u(x)$  denotes the uniform distribution over  $x$ .

we will introduce and evaluate specific indicators that can achieve this purpose with fewer measurements and preparations.

A witness of physical mixture (as opposed to probabilistic) can be evaluated using only measurements of the Pauli observables  $\sigma_x$  on  $C$  and  $\sigma_z$  on  $B$ , with outcomes  $c, b = \pm 1$ , while preparing the  $d$  eigenstate of  $\sigma_y$  on  $D$ , with  $P(d = \pm 1) = \frac{1}{2}$ . (Different choices of Pauli observables generate a family of such witnesses.) For subsets of this data with different values of  $b$ , one can compute the covariance of  $c$  and  $d$ , which we denote  $\text{cov}(c, d|b)$  (see Supplementary Note 5 for details). Letting  $P(b)$  denote the probability of obtaining the outcome  $b$ , we define our

witness to be

$$\mathcal{C}_{CD} \equiv 2 \sum_b b P(b)^2 \text{cov}(cd|b). \quad (4)$$

We show in Supplementary Note 5 that  $\mathcal{C}_{CD} = 0$  for all probabilistic mixtures of common-cause and cause-effect, which implies that  $\mathcal{C}_{CD} \neq 0$  heralds a physical mixture.

We reconstruct the operators  $\tau_{BD}^e$ ,  $\tau_{CB}^d$  and  $\tau_{CD}^b$  using subsets of tomographic data (for example, using only runs that found  $B$  in the state  $|H\rangle$  to reconstruct  $\tau_{CD}^H$ ). The entanglement of these states is quantified by the negativity [24],

$$\mathcal{N}_{XY}^z \equiv \frac{1}{2} (\text{Tr}[T_Y(\tau_{XY}^z)] - 1), \quad (5)$$

where  $T_Y(\cdot)$  denotes transposition on  $Y$ . Quantumness in the cause-effect and common-cause pathways is therefore

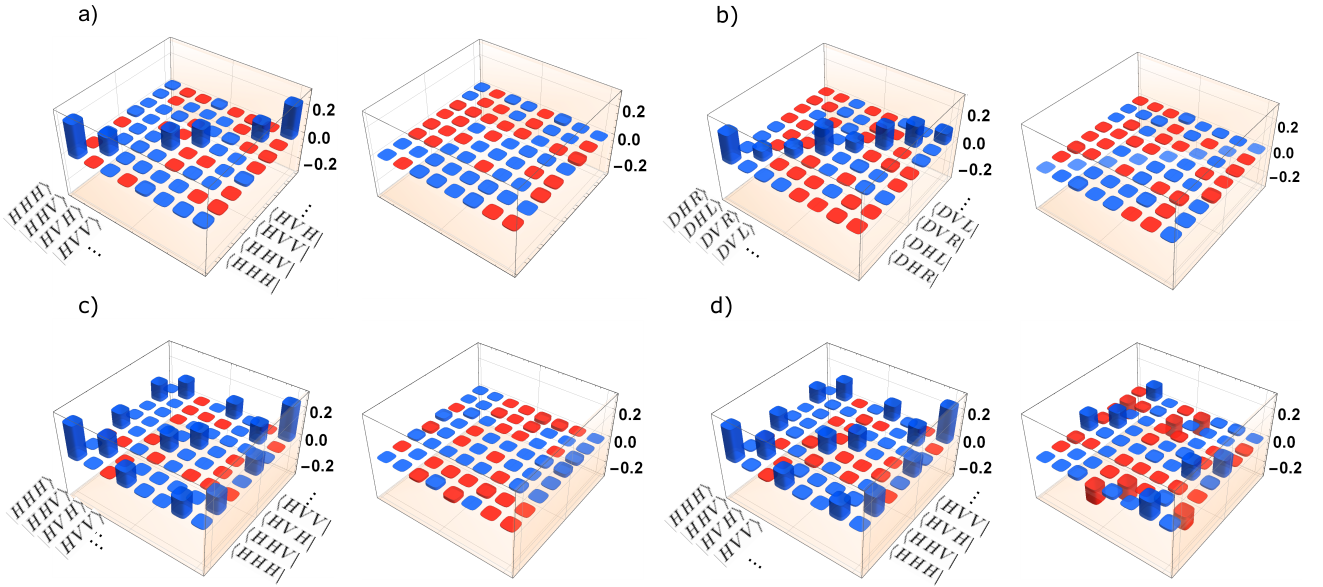
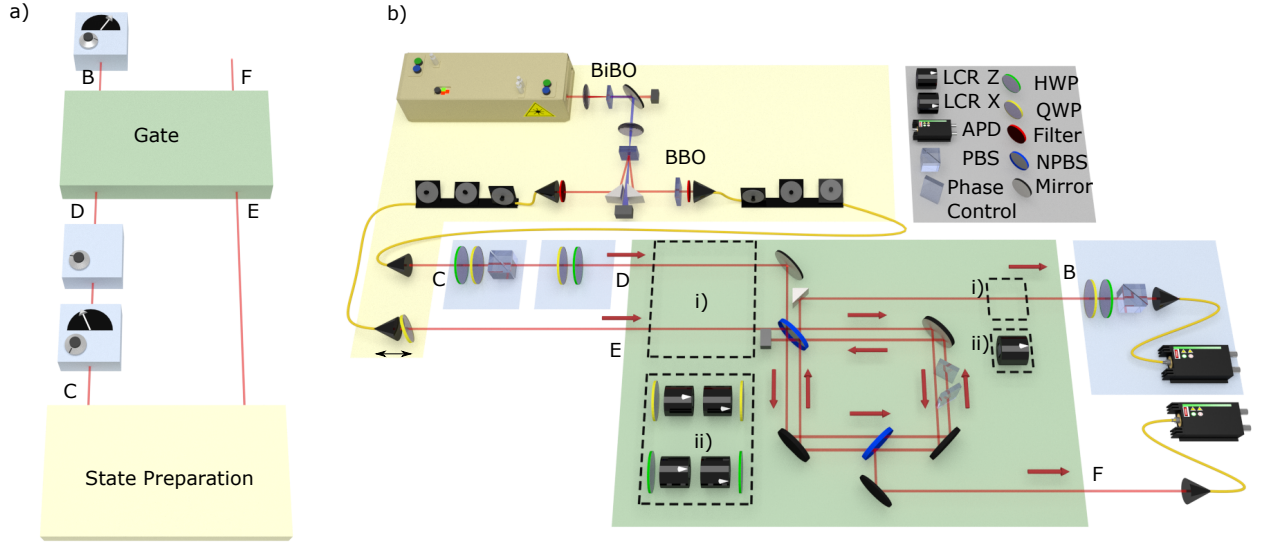
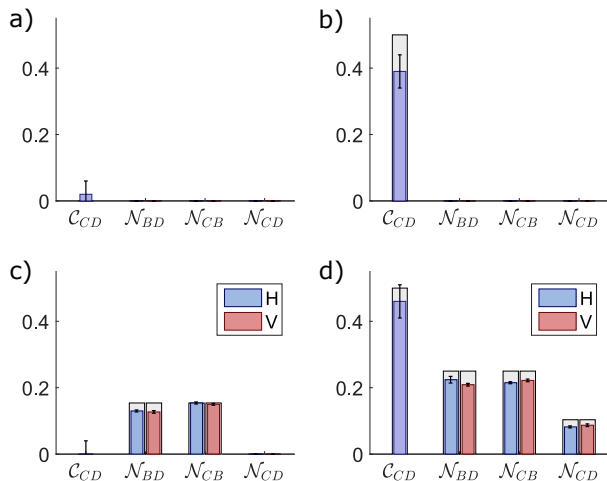


FIG. 6. **Reconstructed causal maps.** Reconstruction of the real and imaginary parts of the Choi state  $\tau_{CBD} = \text{Tr}_{FD'}[(\mathcal{E}_{BF|D'E} \otimes \mathcal{I}_{CD})(|\Phi^+\rangle\langle\Phi^+|_{D'D} \otimes \rho_{CE})]$  when targeting four combinations of cause-effect and common-cause mechanisms: a) PROB C, b) PHYS C, d) PROB Q, d) COH. The causal maps for (a) and (b) are given in the local bases that diagonalize the target map, in order to make explicit their classical nature; no such bases exist for (c) and (d). Blue (red) colour bars represent positive (negative) values. The fidelities [23],  $F \equiv \left[ \text{Tr} \sqrt{\tau^{\frac{1}{2}} \tau_{\text{th}} \tau^{\frac{1}{2}}} \right]^2$ , to the theoretically calculated Choi state  $\tau_{\text{th}}$  are high, at  $(98.1 \pm 0.2)\%$ ,  $(98.06 \pm 0.08)\%$ ,  $(97.1 \pm 0.1)\%$  and  $(93.7 \pm 0.3)\%$ , respectively, verifying that the experiment is performing as intended. Uncertainties on fidelities indicate one standard deviation and are estimated using Monte-Carlo simulations with Poissonian noise on photon counts. Notation for polarization states:  $|H\rangle$ , horizontal,  $|V\rangle$  vertical,  $|D\rangle = 1/\sqrt{2}(|H\rangle + |V\rangle)$  diagonal,  $|A\rangle = 1/\sqrt{2}(|H\rangle - |V\rangle)$  anti-diagonal,  $|R\rangle = 1/\sqrt{2}(|H\rangle + i|V\rangle)$  right-circular,  $|L\rangle = 1/\sqrt{2}(|H\rangle - i|V\rangle)$  left-circular.



**FIG. 7. Classifying causal relations using induced correlations.** For each circuit in Fig. 4, we present theoretical (grey) and experimental (coloured) values for the different witnesses of causal relations. Circuits (b) and (d) have  $\mathcal{C}_{CD} \neq 0$ , witnessing physical mixtures, whereas (a) and (c) are consistent with probabilistic mixtures, since  $\mathcal{C}_{CD}$  is zero within one standard deviation. Circuits (c) and (d) show evidence of intrinsically quantum cause-effect and common cause mechanisms,  $\mathcal{N}_{BD}^c \neq 0$  and  $\mathcal{N}_{CB}^d \neq 0$  for  $d, c = H, V$ , whereas (a) and (b) are consistent with classical mechanisms. Only (d) has  $\mathcal{N}_{CD}^b \neq 0$  for  $b = H, V$ , witnessing a Quantum Berkson Effect. Uncertainties indicate one standard deviation and are estimated using Monte Carlo simulations, assuming Poissonian noise on the photon counts.

witnessed by  $\mathcal{N}_{BD}^c > 0 \forall c$  and  $\mathcal{N}_{CB}^d > 0 \forall d$ , respectively, while  $\mathcal{N}_{CD}^b > 0 \forall b$  witnesses a Quantum Berkson Effect. See Supplementary Note 4 for more details on obtaining the negativity of the pre- and post-selected states from experimental data.

Figure 7 summarizes the values of these witnesses for the four circuits of Fig. 4 along with the corresponding theoretical expectations. The indicators  $\mathcal{N}_{BD}^c$ ,  $\mathcal{N}_{CB}^d$  and  $\mathcal{N}_{CD}^b$  are evaluated using tomographic reconstructions of the operators  $\tau_{BD}^c$ ,  $\tau_{CB}^d$  and  $\tau_{CD}^b$ , respectively, under preparations (on  $D$ ) and measurements (on  $C$  and  $B$ ) of  $\{|H\rangle, |V\rangle\}$ . Scenarios (b) and (d) show evidence of a physical mixture, with  $\mathcal{C}_{CD} = 0.40 \pm 0.02$  and  $\mathcal{C}_{CD} = 0.46 \pm 0.02$  while scenarios (c) and (d) exhibit quantumness in the common-cause and cause-effect pathways. We find  $\mathcal{N}_{CB}^d$  and  $\mathcal{N}_{BD}^c$  non-zero for  $c, d \in \{H, V\}$ . These signatures confirm that we realized physical mixtures and quantum common-cause and cause-effect mechanisms as intended.

The most important indicator for our purposes is  $\mathcal{N}_{CD}^b$ , which verifies the Quantum Berkson Effect. As expected, scenarios (a-c) have  $\mathcal{N}_{CD}^b = 0$  (to within statistical error) and are therefore compatible with an incoherent mixture of common-cause and cause-effect relations. Scenario (d), however, exhibits Berkson-type induced entanglement,

with  $\mathcal{N}_{CD}^H = (0.083 \pm 0.003)$  and  $\mathcal{N}_{CD}^V = (0.087 \pm 0.004)$ . This, combined with the evidence of quantumness of each individual mechanism, constitutes a clear signature of the class COH, a quantum-coherent mixture of cause-effect and common-cause relations.

## DISCUSSION

A priori, it is not obvious how one ought to define a quantum-coherent combination of causal relations, in particular a quantum-coherent combination of common-cause and cause-effect relations. In this article, we have proposed a particular definition and demonstrated the possibility of realizing such quantum-coherence experimentally. There are two distinct notions of quantum coherence that one might think are pertinent to our problem, and both feature in our definition.

The first notion of quantum coherence applies to elements of a set of alternatives that are jointly exhaustive and mutually exclusive, such as the eigenstates of some observable. In this case, an incoherent mixture is a probabilistic mixture of the alternatives and consequently it is reasonable to define a state as exhibiting coherence whenever it cannot be expressed as such a probabilistic mixture. However, the sorts of causal relations that we here seek to combine coherently, a cause-effect relation and a common-cause relation, do not constitute mutually exclusive alternatives. A pair of systems may be connected by both a cause-effect relation and a common cause. The possibility of two causal mechanisms acting simultaneously necessitates the category of physical mixtures of causal mechanisms. Given that such physical mixtures can arise classically, the mere inapplicability of a probabilistic mixture should not lead one to infer the presence of quantumness. This is why we use additional criteria for judging a combination of causal relations to be a quantum-coherent combination. Because physical mixtures are distinguished by the strength of the induced correlations in the Berkson effect, we have proposed that a necessary condition for having a quantum-coherent mixture is that the Berkson-induced correlations exhibit entanglement.

The second notion of quantum coherence is the one relative to which different systems are said to be coherent with one another: for independent systems, this occurs when their joint state is entangled, for the input and output of a quantum channel, this occurs when the channel is not entanglement-breaking. In the causal context, therefore, a common-cause relation between a pair of systems can be judged coherent if the state of the systems is entangled, while a cause-effect relation between a pair of systems can be judged coherent if the associated channel is not entanglement breaking. This second notion of coherence is applicable, therefore, to individual causal pathways rather than the manner in



which they are combined. Consequently, we have proposed that another necessary condition for a mixture of cause-effect and common-cause relations to be quantum-coherent is that each of the pathways, common-cause and cause-effect, are themselves coherent.

Our approach to defining quantum-coherent combinations of different causal relations differs significantly from the one suggested in recent work seeking to define superpositions of different causal orders. The proposal for witnessing causal nonseparability in Ref. [25], for instance, judges the causal order between a pair of systems to be quantum-indefinite whenever the causal map cannot be written as a probabilistic mixture of terms with definite causal orders. However, from our perspective,  $A$  causing  $B$  is not necessarily mutually exclusive to  $B$  causing  $A$  (just as a common-cause relation is not mutually exclusive to a cause-effect relation). To imagine both acting simultaneously – which we would term a physical mixture of the two cause-effect relations – is simply to imagine the possibility of causal cycles. This is an exotic possibility, but one that is classically meaningful. As such, having a causal map that is not a probabilistic mixture of causal orders need not, by itself, be evidence of quantumness. See Supplementary Discussion 1 for more on the related topic of superposition of causal orders.

As we progress to studying more complex scenarios, for instance, involving a larger number of systems, we are likely to find an even wider range of types of coherence, resembling the many types of entanglement that arise when more than two parties are involved. The problem of classifying the causal possibilities in this case—in particular quantum-coherent mixtures of various relations—is significantly more complex than the one considered here. Developing such a classification for an arbitrary number of systems with arbitrary dimensionality constitutes an important pillar in the new research programme that seeks to understand causality in quantum theory.

The understanding of new, uniquely quantum, combinations of common-cause and cause-effect relations introduced in this article also has implications for the topic of non-Markovianity. In the context of the dynamics of open quantum systems, the assumption of Markovianity states that the environment with which the principal system interacts has no memory and hence is unable to preserve a record of earlier states of the system. (See Ref. [26, 27] for a review of proposed quantum statements of Markovianity.) This assumption simplifies the mathematical treatment of the system’s dynamics considerably, but in most realistic models it holds only approximately, which has sparked considerable interest in quantum non-Markovianity in recent years. From the perspective of causal modeling, non-Markovianity arises when the environment acts as a common cause of the system at different times (in addition to the cause-effect relations arising from the evolution of the system itself).

As such, the fact that there are intrinsically quantum ways of mixing common-cause and cause-effect relations implies a greater variety of types of non-Markovianity than one sees classically.

## METHODS

### Photon Source

We produce polarization entangled photon pairs using spontaneous parametric downconversion in two type-I nonlinear crystals. We begin with a Ti:Sapphire laser, centred at 790 nm with a spectral bandwidth of 10.5nm, a repetition rate of 80 MHz, and an average power of 2.65 W. The laser light is frequency doubled in a 2-mm thick bismuth-borate (BiBO) crystal, which creates a pump beam of 0.65 W centred at 395nm with a 1 nm FWHM bandwidth. With two cylindrical lenses, the pump is focused onto a pair of 1 mm  $\beta$ -barium-borate (BBO) crystals with orthogonal orientations for type-I spontaneous parametric downconversion. Bandpass filters are placed to reduce background noise from the pump. Additional compensation crystals are used in order to counteract the effects of temporal and spatial walkoff [28]. Polarization entangled photon pairs at 790 nm are prepared in the state  $|\Phi^+\rangle$ , which we achieve with  $(96.31 \pm 0.08)\%$  fidelity. Inteferece filters on both sides set the photon bandwidths to 3nm. The photons are then coupled into single mode fibres and sent towards the partial swap. The polarization is set with polarization controllers and the phase of the entangled state is tuned by tilting a quarter-wave plate (QWP) at the output of one of the fibres.

### Implementing the partial swap

The partial swap uses a folded displaced Sagnac interferometer, with two 50/50 beam splitters and two NBK-7 glass windows, which are counter rotated in order to set the phase with minimal beam deflection. The visibility of the Sagnac interferometer without background subtraction is  $(93.6 \pm 0.1)\%$ . This is measured by blocking one input ( $D$  or  $E$ ) to the gate and measuring the number of photons at the output  $B$  as a function of the window angles in the Sagnac interferometer. For the coherent partial swap to be effective, photon pairs in modes  $D$  and  $E$  must undergo two-photon quantum interference on a beam splitter prior to entering the gate. Hong-Ou-Mandel (HOM) interference between photons input at  $D$  and  $E$  is measured at the first beam splitter using a translation stage on input  $E$ . A dip in visibility of  $(95 \pm 2)\%$  is achieved. To implement the gate for the class PROBQ, a delay of 3 ps is added to photon  $E$  which removes the interference. For all other cases, the delay is set to a value

corresponding to the centre of the HOM dip to maximize the two photon interference.

### Dephasing Channels

The dephasing channels before and after the Sagnac interferometer are implemented using variable liquid crystal retarders (LCR), which exhibit a voltage dependent birefringence, introducing a relative phase of 0 or  $\pi$  on orthogonal polarization states. Probabilistic dephasing is achieved by switching them on and off at random at a rate of 10 Hz, with probability 1/2 of implementing a  $\pi$  phase shift during each interval. The input and outputs can be dephased on a different polarization bases. Dephasing along the  $\{|D\rangle, |A\rangle\}$  basis is achieved with the LCR axis at  $0^\circ$ , and in the  $\{|H\rangle, |V\rangle\}$  basis at  $45^\circ$ . Two quarter-wave plates on either side of the LCR after  $D$  and two half-wave plates on either side of the LCR after  $E$  are used to rotate between the different dephasing bases required for the classical mixtures.

### Measurement Procedure

The experiment proceeds in the following way. The unitary  $U_{BF|DE}$  is set by adjusting the window angles in the Sagnac interferometer such that the phase difference between the two paths is  $\pi/2$ . A HOM dip is then measured and the arrival time of the photons is set with a translation stage at  $E$ . The entangled state on  $C$  and  $E$  is initialized by preparing and measuring remote entanglement between  $C$  and  $B$ . The polarization is measured using a half-wave plate (HWP), quarter-wave plate (QWP), and polarizing beam splitter (PBS) in sequence. The HWP and QWP are adjusted so that one polarization state can pass through the PBS. The polarization at  $C$  is measured with a HWP and QWP, and assuming the photon has passed through the PBS, the polarization is reprepared with another QWP and HWP at  $D$ . Photons are then sent to the partial swap gate, and the polarization at  $B$  is measured using another QWP and HWP. Coincidence counts at  $F$  and  $B$  are measured using Silicon avalanche photodiodes and a coincidence logic with a coincidence window of 3 ns. Coincidences are measured at a rate of approximately 1 kHz. We measure the different combinations of polarization eigenstates and repeat the procedure for the four different causal scenarios.

**Acknowledgments** This research was supported in part by the Foundational Questions Institute (grant number FQXI-RFP-1516), the Natural Sciences and Engineering Research Council of Canada (NSERC), Canada Research Chairs, Industry Canada and the Canada Foundation for Innovation (CFI). Research at Perimeter Institute is supported by the Government of Canada through

Industry Canada and by the Province of Ontario through the Ministry of Research and Innovation.

**Contributions** RWS, KR and KJR conceived the original idea for the project. KR and RWS developed the project and the theory. JPWM and KJR designed the experiment. JPWM performed the experiment and the numerical calculations. JPWM, KR, RWS and KJR analyzed the results. JPWM and KR wrote the first draft of the paper and all authors contributed to the final version.

**Corresponding author** Correspondence and request for materials should be addressed to J.P.W.M. (jpmaclean@uwaterloo.ca) or K.R. (katja.ried@uibk.ac.at).

### REFERENCES

- [1] J. Pearl, *Causality: models, reasoning and inference* (Cambridge Univ. Press, New York, 2000).
- [2] P. Spirtes, C. Glymour, and R. Scheines, *Causation, prediction, and search* (MIT Press, Cambridge, 2000).
- [3] T. Fritz, New J. Phys. **14**, 103001 (2012).
- [4] C. J. Wood and R. W. Spekkens, New Journal of Physics **17**, 033002 (2015).
- [5] R. Chaves, L. Luft, and D. Gross, New Journal of Physics **16**, 043001 (2014).
- [6] R. Chaves, C. Majenz, and D. Gross, Nature Communications **6**, 5766 (2015).
- [7] F. Markopoulou and L. Smolin, Phys. Rev. D **58**, 084032 (1998).
- [8] L. Hardy, Journal of Physics A: Mathematical and Theoretical **40**, 3081 (2007).
- [9] K. Ried, M. Agnew, L. Vermeyden, D. Janzing, R. W. Spekkens, and K. J. Resch, Nat. Phys. **11**, 414 (2015).
- [10] M. S. Leifer, Phys. Rev. A **74**, 042310 (2006).
- [11] Y. Aharonov, S. Popescu, J. Tollaksen, and L. Vaidman, Phys. Rev. A **79**, 052110 (2009).
- [12] G. Chiribella, G. M. D'Ariano, and P. Perinotti, Phys. Rev. A **80**, 022339 (2009).
- [13] L. Hardy, Philos. T. Roy. Soc. A **370**, 3385 (2012).
- [14] O. Oreshkov, F. Costa, and C. Brukner, Nat. Commun. **3**, 1092 (2012).
- [15] J. Fitzsimons, J. Jones, and V. Vedral, arXiv:1302.2731 (2013).
- [16] M. Leifer and R. W. Spekkens, Phys. Rev. A **88**, 052130 (2013).
- [17] G. Chiribella, Phys. Rev. A **86**, 040301 (2012).
- [18] L. Hardy, "Quantum gravity computers: On the theory of computation with indefinite causal structure," (2007).
- [19] M. Araújo, F. Costa, and v. Brukner, Phys. Rev. Lett. **113**, 250402 (2014).
- [20] L. M. Procopio, A. Moqanaki, M. Araújo, F. Costa, I. A. Calafell, E. G. Dowd, D. R. Hamel, L. A. Rozema, Časlav Brukner, and P. Walther, Nat. Commun. **6**, 7913 (2015).
- [21] M. D. Choi, Linear Algebra Appl. **10**, 285 (1975).
- [22] A. Černoch, J. Soubusta, L. Bartůšková, M. Dušek, and J. Fiurásek, Phys. Rev. Lett. **100**, 180501 (2008).
- [23] R. Jozsa, Journal of Modern Optics **41**, 2315 (1994).
- [24] G. Vidal and R. F. Werner, Phys. Rev. A **65**, 032314 (2002).

- [25] M. Araújo, C. Branciard, F. Costa, A. Feix, C. Giarlatzi, and Časlav Brukner, *New Journal of Physics* **17**, 102001 (2015).
- [26] Ángel Rivas, S. F. Huelga, and M. B. Plenio, *Reports on Progress in Physics* **77**, 094001 (2014).
- [27] B. Vacchini, A. Smirne, E.-M. Laine, J. Piilo, and H.-P. Breuer, *New J. Phys.* **13**, 093004 (2011).
- [28] J. Lavoie, R. Kaltenbaek, and K. J. Resch, *New Journal of Physics* **11**, 073051 (2009).
- [29] A. Jamiolkowski, *Rep. Math. Phys.* **3**, 275 (1972).
- [30] D. F. V. James, P. G. Kwiat, W. J. Munro, and A. G. White, *Physical Review A* **64**, 052312 (2001).
- [31] T. M. Cover and J. A. Thomas, *Elements of information theory* (Wiley, 2006).
- [32] G. Chiribella, G. M. D'Ariano, P. Perinotti, and B. Valiron, *Phys. Rev. A* **88**, 022318 (2013).

## SUPPLEMENTARY NOTES

### Supplementary Note 1: Probabilistic mixtures of common-cause and cause-effect relations

As defined in the main text of the article, a causal map  $\mathcal{E}_{CB|D}$  is said to physically realize a probabilistic mixture of cause-effect and common-cause relations if it is possible to express it as follows: there is a hidden classical control variable,  $J$ , which only influences  $B$ , such that for every value of  $J$ , either  $B$  depends only on  $D$  in the causal map or  $B$  depends only on its common cause with  $C$ . In this section, we discuss why this is the appropriate notion of probabilistic mixture to study. We also demonstrate that it implies that the causal map has the form

$$\mathcal{E}_{CB|D} = w\mathcal{E}_{B|D} \otimes \rho_C + (1-w)\rho_{CB} \otimes \text{Tr}_D, \quad (6)$$

where  $0 \leq w \leq 1$  and

$$\text{Tr}_B \rho_{CB} = \rho_C. \quad (7)$$

We are here concerned with what sorts of probabilistic mixtures of causal structures are physically realizable. Note that a probabilistic mixture of alternatives is always physically realized by making the choice of alternatives depend causally on the value of a control variable that has been sampled from some probability distribution and for which the value is not observed. It follows that to be physically realizable, a probabilistic mixture of the elements of a set of causal maps,  $\{\mathcal{E}_{CB|D}^{(j)}\}$ , must have the form  $\mathcal{E}_{CB|D} = \sum_j P(j)\mathcal{E}_{CB|D}^{(j)}$ , where  $J$  denotes the hidden control variable and  $P(j)$  is the probability that  $J = j$ .

What is critical to recognize is that the causal dependence of systems on the control variable cannot be treated abstractly but must instead be considered as part of the causal structure. One can then ask whether one can infer any constraints on the causal structure of the

probabilistic mixture from the causal structure of the elements appearing in the mixture. We argue that there is indeed a very natural constraint:

If all of the causal maps in a probabilistic mixture describe the same causal relation, then their mixture should describe this causal relation as well.

Note, first of all, that one particular implication of this constraint is that a causal map that is a probabilistic mixture of purely cause-effect maps should be purely cause-effect. We now demonstrate how this constraint implies a restriction on the sorts of probabilistic mixtures that can be physically realized.

To begin, we consider the possibility that the set of probabilistic mixtures of causal structures that are physically realizable is the full set of such mixtures. In this case, the causal maps corresponding to physically-realizable probabilistic mixtures of cause-effect and common-cause relations would be those that are a convex sum of causal maps each of which is purely cause-effect or purely common-cause, that is, those of the form

$$\mathcal{E}_{CB|D} = \sum_{j \in \mathcal{J}_1} P(j)\mathcal{E}_{B|D}^{(j)} \otimes \rho_C^{(j)} + \sum_{j \in \mathcal{J}_2} P(j)\rho_{CB}^{(j)} \otimes \text{Tr}_D, \quad (8)$$

where the set of values of  $J$  are partitioned into two subsets, denoted  $\mathcal{J}_1$  and  $\mathcal{J}_2$ , and  $P$  is a probability distribution thereon.

In order to realize such a causal map, the control variable  $J$  needs to have a causal influence on both  $B$  and  $C$ . Otherwise, we could not explain how the marginal states on  $B$  and on  $C$  both vary with the value of  $J$ . In this case,  $J$  acts as a common cause of  $B$  and  $C$ , and the causal structure of the overall causal map is that of 8(a).

The alternative proposal, the one that we endorse here, is that the control variable  $J$  only has a causal influence on  $B$ . In this case, the causal structure of the overall causal map is that of 8(b).

We now demonstrate that the assumption that  $J$  is a cause of both  $B$  and  $C$  violates the natural constraint articulated above. Consider first the implication of the constraint for probabilistic mixtures of purely cause-effect maps. If every map in the probabilistic mixture is purely cause-effect, then for all values  $j$  of  $J$ ,  $\mathcal{E}_{CB|D}^{(j)} = \mathcal{E}_{B|D}^{(j)} \otimes \rho_C^{(j)}$ . The fact that  $J$  can influence  $B$  and  $C$  is encoded here in the fact that the marginal on  $C$  is  $j$ -dependent. But now consider the causal map associated to this probabilistic mixture. It is  $\mathcal{E}_{CB|D} = \sum_j w_j \mathcal{E}_{B|D}^{(j)} \otimes \rho_C^{(j)}$ . This is not a purely cause-effect map in general because, by definition, such maps must take the form of a tensor product of a map from  $D$  to  $B$  and a state on  $C$ . We can understand this by noting that the control variable acts as a common cause, so

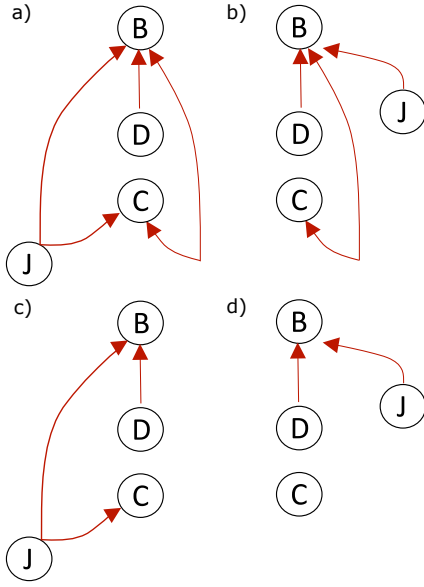


FIG. 8. **a)** Causal relations between  $A$  (split into  $C$  and  $D$ ) and  $B$  where the control variable  $J$  acts as a common cause for both  $B$  and  $C$ . **b)** We propose that a causal map represents a probabilistic mixture of common-cause and cause-effect if it is possible to achieve it by a hidden control variable  $J$  acting only on  $B$ . **c,d)** If one mixes only cause-effect relations, then the result, according to our constraint, should also be purely cause-effect. Again, this condition is not satisfied if the control variable  $J$  acts as a common cause of  $B$  and  $C$ , but it is if  $J$  influences only  $B$ .

that the causal structure is that depicted in 8(c), which is clearly not purely cause-effect. Thus if one demands that any physical realization of a probabilistic mixture of purely cause-effect maps should itself be purely cause-effect, the scheme just described does not in fact realize such a mixture.

On the other hand, if we demand that  $J$  can only influence  $B$ , as in 8(d), then  $\mathcal{E}_{CB|D} = \left(\sum_j \mathcal{E}_{B|D}^{(j)}\right) \otimes \rho_C$ . Here the marginal on  $C$  is  $j$ -independent and therefore can be factorized out of the sum. This is a purely cause-effect map, and so the constraint is satisfied.

We now show how to prove that all physically-realizable probabilistic mixtures can be expressed as a probabilistic mixture of just two causal maps, one of which is purely cause-effect and the other of which is purely common-cause.

By our definition, it must be possible to partition the values of  $J$  into two subsets, denoted  $\mathcal{J}_1$  and  $\mathcal{J}_2$ , where for  $j \in \mathcal{J}_1$ ,  $B$  depends only on  $D$ , so that  $\mathcal{E}_{CB|D}^{(j)} = \mathcal{E}_{B|D}^{(j)} \otimes \rho_C$ , and where for  $j \in \mathcal{J}_2$ ,  $B$  depends only on the common cause with  $C$ , so that  $\mathcal{E}_{CB|D}^{(j)} = \rho_{CB}^{(j)} \otimes \text{Tr}_D$ . The fact that the control variable  $J$  is assumed to have no influence on  $C$  implies that for all values of  $J$ , the causal map  $\mathcal{E}_{CB|D}^{(j)}$  must have the same marginal on  $C$ . This is why  $\rho_C$  has no dependence on  $j$  in the expression for  $\mathcal{E}_{CB|D}^{(j)}$  when

$j \in \mathcal{J}_1$ . The lack of influence of  $J$  on  $C$  also implies that we must have

$$\text{Tr}_B \rho_{CB}^{(j)} = \rho_C, \quad (9)$$

for all  $j \in \mathcal{J}_2$ .

The overall causal map is obtained by weighting the  $\mathcal{E}_{CD|D}^{(j)}$  by the probability  $P(j)$  of their occurrence, so that

$$\mathcal{E}_{CB|D} = \sum_{j \in \mathcal{J}_1} P(j) \mathcal{E}_{B|D}^{(j)} \otimes \rho_C + \sum_{j \in \mathcal{J}_2} P(j) \rho_{CB}^{(j)} \otimes \text{Tr}_D.$$

Finally, defining

$$w \equiv \sum_{j \in \mathcal{J}_1} P(j),$$

and

$$\mathcal{E}_{B|D} \equiv \frac{1}{w} \sum_{j \in \mathcal{J}_1} P(j) \mathcal{E}_{B|D}^{(j)},$$

and

$$\rho_{CB} \equiv \frac{1}{1-w} \sum_{j \in \mathcal{J}_2} P(j) \rho_{CB}^{(j)}, \quad (10)$$

we obtain supplementary equation 6. Supplementary equation 10 together with supplementary equation 9 implies supplementary equation 7.

### Supplementary Note 2: The Choi isomorphism and different classes of causal maps

We begin by introducing a useful tool for defining and characterizing causal maps that puts quantum channels, viz completely positive and trace-preserving (CPTP) maps, on an equal footing with bipartite quantum states. The Choi isomorphism [21] (see also [29]) establishes that completely positive maps from linear operators on the Hilbert space of  $A$  to linear operators on  $B$ , denoted  $\mathcal{E}_{B|A} : \mathcal{L}(\mathcal{H}_A) \rightarrow \mathcal{L}(\mathcal{H}_B)$ , are isomorphic to positive-semidefinite operators  $\tau_{BA} \in \mathcal{H}_B \otimes \mathcal{H}_A$  given by

$$\tau_{BA} \equiv (\mathcal{E}_{B|A'} \otimes \mathbb{1}_A) (|\Phi^+\rangle \langle \Phi^+|_{A'A}). \quad (11)$$

Here,  $|\Phi^+\rangle_{A'A} = \frac{1}{\sqrt{d}} \sum_{k=1}^d |k\rangle_{A'} |k\rangle_A$  denotes the symmetric, maximally entangled state between  $A$  and an ancilla,  $A'$ , where  $d$  is the Hilbert space dimension of  $A$  and  $A'$ . (Different choices of  $\{|k\rangle\}$  lead to different forms of the Choi state; we will fix a convention for our calculations below.) Note that the different subscript in  $\mathcal{E}_{B|A'}$  indicates that the map is acting on input  $A'$  and taking it to output  $B$ , as shown in 9. Since  $|\Phi^+\rangle$  is normalized,  $\tau_{BA}$  also has unit trace, making it a valid quantum state,

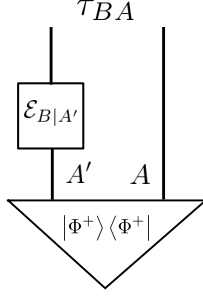


FIG. 9. Operational interpretation of the Choi state  $\tau_{BA}$ . It can be prepared by starting with the maximally entangled state  $|\Phi^+\rangle$  on  $A$  and  $A'$  and applying the map to  $A'$ .

if the map is trace-preserving. We refer to  $\tau_{BA}$  as the Choi state of the map  $\mathcal{E}_{B|A}$ .

The isomorphism also allows us to express the effect of the map on a generic input in terms of its Choi state [16]: for any linear operator  $\rho_A$  on  $\mathcal{H}_A$ ,

$$\begin{aligned} \mathcal{E}_{B|A}(\rho_A) &= d \operatorname{Tr}_A [(T_A \tau_{BA}) \mathbb{1}_B \otimes \rho_A] \\ &= d \operatorname{Tr}_A [\tau_{BA} \cdot (\mathbb{1}_B \otimes T_A \rho_A)]. \end{aligned} \quad (12)$$

The transposition on  $A$ , denoted  $T_A$ , must be included in this expression in order for  $\tau_{BA}$  to be a positive operator. It can be applied either to the input  $\rho_A$  or to the Choi state itself. The identity operator on  $B$ , which is formally required in order for us to multiply  $\tau_{BA}$  and  $\rho_A$ , is often omitted in the following for brevity.

#### Example classes of causal maps

In the following section, we show how the circuits presented in Fig. 4 realize examples of the causal maps  $\mathcal{E}_{CB|D}$  in the classes COH (hence PHYSQ), PROBQ, PROBC, and PHYSC, respectively. In each case, we begin with a specification of the circuit elements, namely the state  $\rho_{CE}$ , which will be taken to be the maximally entangled state  $|\Phi^+\rangle$  in all following cases, and the gate  $\mathcal{E}_{BF|DE}$ , and find the causal map via

$$\mathcal{E}_{CB|D}(\cdot) = \operatorname{Tr}_F \circ \mathcal{E}_{BF|DE}(\cdot \otimes \rho_{CE}). \quad (13)$$

We then derive the associated Choi state,  $\tau_{CBD} \in \mathcal{L}(\mathcal{H}_C \otimes \mathcal{H}_B \otimes \mathcal{H}_D)$ , which is given by

$$\begin{aligned} \tau_{CBD} &= (\mathcal{E}_{CB|D'} \otimes \mathcal{I}_D) (|\Phi^+\rangle \langle \Phi^+|_{D'D}) \\ &= \frac{1}{2} \sum_{j,k} \mathcal{E}_{CB|D'} (|j\rangle \langle k|_{D'}) \otimes |j\rangle \langle k|_D, \end{aligned} \quad (14)$$

and use the witnesses introduced in the main paper to classify the corresponding causal maps. We will take the basis  $|H\rangle, |V\rangle$  of eigenstates of the Pauli operator  $\sigma_z$

(which corresponds to horizontal and vertical polarization states) as the basis defining the Choi isomorphism; that is,

$$|\Phi^+\rangle \equiv \frac{1}{\sqrt{2}}(|HH\rangle + |VV\rangle). \quad (15)$$

#### Example of COH

We begin with the circuit in Fig. 4(d), which realizes an example of COH. The circuit applies the partial swap gate from equation 2,

$$\mathcal{E}_{BF|DE}(\cdot) = U_{BF|DE}(\cdot) U_{BF|DE}^\dagger, \quad (16)$$

where

$$U_{BF|DE} = \frac{1}{\sqrt{2}} \mathbb{1}_{B|D} \otimes \mathbb{1}_{F|E} + \frac{i}{\sqrt{2}} \mathbb{1}_{B|E} \otimes \mathbb{1}_{F|D}. \quad (17)$$

The first term of supplementary equation 17 corresponds to the identity operation, which maps  $D$  to  $B$  and  $E$  to  $F$ , and the second term corresponds to the swap operation, which maps  $D$  to  $F$  and  $E$  to  $B$ .

Inserting supplementary equation 16 and supplementary equation 17 as well as equation 1 from the main text into supplementary equation 13, one can find an explicit expression for the causal map realized by the partial swap,  $\mathcal{E}_{CB|D}^{coh}$ . However, in order to derive the compact expression quoted in the main text (equation 3), we will consider a Kraus representation of the map: a set of operators  $W_k$  such that

$$\mathcal{E}_{CB|D}^{coh}(\cdot) = \sum_k W_k(\cdot) W_k^\dagger. \quad (18)$$

One possible choice of Kraus operators is given in terms of the unitary that defines  $\mathcal{E}_{BF|DE}$  by

$$W_k = \langle k_F | U_{BF|DE} | \Phi^+ \rangle_{CE}, \quad (19)$$

where  $\{|k\rangle\}$  is an arbitrary orthonormal basis of the Hilbert space of  $F$ .

We take  $k \in \{H, V\}$ , ranging over eigenvectors of  $\sigma_z$ , which is the same basis that puts the initial state of  $CE$  in a simple form. Substituting supplementary equation 17, we obtain

$$\begin{aligned} W_k &= \sum_{m \in \{H, V\}} \langle k_F | U_{BF|DE} | mm \rangle_{CE} \\ &= \sum_{m \in \{H, V\}} \frac{1}{\sqrt{2}} \langle k_F | \mathbb{1}_{B|D} \otimes \mathbb{1}_{F|E} | mm \rangle_{CE} \\ &\quad + \frac{i}{\sqrt{2}} \langle k_F | \mathbb{1}_{B|E} \otimes \mathbb{1}_{F|D} | mm \rangle_{CE} \\ &= \frac{1}{\sqrt{2}} (A_k + iB_k), \end{aligned} \quad (20)$$

where we introduce the components

$$\begin{aligned} A_k &\equiv \sum_{m \in \{H, V\}} \frac{1}{\sqrt{2}} \langle k_F | \mathbb{1}_{B|D} \otimes \mathbb{1}_{F|E} |mm\rangle_{CE} \\ &= \frac{1}{\sqrt{2}} \mathbb{1}_{B|D} \otimes |k\rangle_C \end{aligned} \quad (21)$$

$$\begin{aligned} B_k &\equiv \sum_{m \in \{H, V\}} \frac{1}{\sqrt{2}} \langle k_F | \mathbb{1}_{B|E} \otimes \mathbb{1}_{F|D} |mm\rangle_{CE} \\ &= |\Phi^+\rangle_{CB} \langle k|_D. \end{aligned} \quad (22)$$

Note that the  $A_k$  contain only the two-qubit identity operator, which we expect to implement a purely cause-effect relation (the first term in supplementary equation 17), whereas the  $B_k$  contain only the swap operator, which we expect to realize a purely common-cause relation (the second term in supplementary equation 17).

In terms of the  $A_k$  and  $B_k$ , we have

$$\begin{aligned} \mathcal{E}_{CB|D}^{coh}(\cdot) &= \sum_k \frac{1}{2} (A_k + iB_k)(\cdot) (A_k + iB_k)^\dagger \\ &= \sum_k \frac{1}{2} A_k(\cdot) A_k^\dagger + \frac{1}{2} B_k(\cdot) B_k^\dagger \\ &\quad - \frac{i}{2} \left\{ A_k(\cdot) B_k^\dagger - B_k(\cdot) A_k^\dagger \right\}. \end{aligned} \quad (23)$$

The effect of the first term is

$$\begin{aligned} \sum_k A_k(\cdot) A_k^\dagger &= \frac{1}{2} \sum_k |k\rangle \langle k|_C \otimes \mathbb{1}_{B|D}(\cdot) \mathbb{1}_{B|D}^\dagger \\ &= \frac{1}{2} \mathbb{1}_C \otimes \mathcal{I}_{B|D}(\cdot) \equiv \mathcal{E}_{CB|D}^{ce}(\cdot), \end{aligned} \quad (24)$$

that is, it applies the identity channel from  $D$  to  $B$ , which is our example of a purely cause-effect relation. The effect of the second term is

$$\begin{aligned} \sum_k B_k(\cdot) B_k^\dagger &= |\Phi^+\rangle \langle \Phi^+|_{CB} \otimes \sum_k \langle k_D | (\cdot) |k_D\rangle \\ &= |\Phi^+\rangle \langle \Phi^+|_{CB} \text{Tr}_D(\cdot) \equiv \mathcal{E}_{CB|D}^{cc}(\cdot), \end{aligned} \quad (25)$$

that is, it traces out  $D$  and prepares the state  $|\Phi^+\rangle$  on  $CB$ , which is our example of a purely common-cause relation. Finally, the cross terms take the form

$$\begin{aligned} &-\frac{i}{2} \sum_k \left\{ A_k(\cdot) B_k^\dagger - B_k(\cdot) A_k^\dagger \right\} \\ &= -\frac{i}{2} \sum_k \left\{ \left( \frac{1}{\sqrt{2}} |k\rangle_C \otimes \mathbb{1}_{B|D} \right) (\cdot) \left( \langle \Phi^+ |_{CB} \otimes \langle k|_D \right) \right. \\ &\quad \left. - \left( |\Phi^+\rangle_{CB} \otimes \langle k|_D \right) (\cdot) \left( \frac{1}{\sqrt{2}} \langle k|_C \otimes \mathbb{1}_{B|D} \right) \right\} \\ &= -i \left[ \frac{1}{2} \mathbb{1}_C \otimes \mathcal{I}_{B|D}(\cdot) \right] |\Phi^+\rangle \langle \Phi^+|_{CB} \\ &\quad + i |\Phi^+\rangle \langle \Phi^+|_{CB} \left[ \frac{1}{2} \mathbb{1}_C \otimes \mathcal{I}_{B|D}(\cdot) \right], \end{aligned} \quad (26)$$

which completes the derivation of equation 3 in the main paper.

The Choi representation of this causal map is then calculated using supplementary equation 14,

$$\begin{aligned} \tau_{CBD}^{coh} &= \frac{1}{2} \left( \frac{1}{2} \mathbb{1}_C \otimes |\Phi^+\rangle \langle \Phi^+|_{BD} \right) + \frac{1}{2} \left( |\Phi^+\rangle \langle \Phi^+|_{CB} \otimes \frac{1}{2} \mathbb{1}_D \right) \\ &\quad - \frac{i}{2} \left\{ \left( \mathbb{1}_C \otimes |\Phi^+\rangle \langle \Phi^+|_{BD} \right) \cdot \left( |\Phi^+\rangle \langle \Phi^+|_{CB} \otimes \mathbb{1}_D \right) \right. \\ &\quad \left. - \left( |\Phi^+\rangle \langle \Phi^+|_{CB} \otimes \mathbb{1}_D \right) \cdot \left( \mathbb{1}_C \otimes |\Phi^+\rangle \langle \Phi^+|_{BD} \right) \right\}. \end{aligned} \quad (27)$$

The Choi state in supplementary equation 27 contains all the information required to characterize the causal structure. In order to evaluate our witnesses, we will calculate the induced states associated with finding certain states on  $C$ ,  $B$  or  $D$ . Letting  $\Pi^b$  denote the projector associated with an eigenvalue  $b$  in a particular measurement on system  $B$ , we use

$$\tau_{CD}^b = \frac{1}{\text{Tr} [\Pi_B^b \cdot \tau_{CBD}^{coh}]} \text{Tr}_B [\Pi_B^b \cdot \tau_{CBD}^{coh}], \quad (28)$$

and similarly for a projector  $\Pi^c$  on  $C$ ,

$$\tau_{BD}^c = \frac{1}{\text{Tr} [\Pi_C^c \cdot \tau_{CBD}^{coh}]} \text{Tr}_C [\Pi_C^c \cdot \tau_{CBD}^{coh}]. \quad (29)$$

The expression for the induced state on  $CB$  generated by an input  $\Pi^d$  on  $D$  differs from the above by a partial transpose, and the renormalization factor to ensure unit trace is always  $d_D$ :

$$\tau_{CB}^d = \mathcal{E}_{CB|D}^{coh}(\Pi_D^d) = d_D \text{Tr}_D [\tau_{CBD}^{coh} T_D(\Pi_D^d)]. \quad (30)$$

If one prepares  $D$  in the state  $|H\rangle$ , then the state on  $CB$  is  $\tau_{CB}^H = \frac{3}{4} |\psi\rangle \langle \psi| + \frac{1}{4} |VH\rangle \langle VH|$  where  $|\psi\rangle = \frac{2}{\sqrt{6}} |HH\rangle + e^{i\pi/4} \frac{1}{\sqrt{3}} |VV\rangle$ , and one can see that  $\tau_{CB}^H$  is entangled. The same holds if one prepares  $|V\rangle$  on  $D$  instead. The causal map  $\mathcal{E}_{CB|D}^{coh}$  is therefore quantum in the cause-effect pathway. If one measures  $C$  and selects for the state  $|H\rangle$ , the resulting map from  $D$  to  $B$  is Choi-isomorphic (up to normalization) to the state  $\tau_{BD}^H = \frac{3}{4} |\tilde{\psi}\rangle \langle \tilde{\psi}| + \frac{1}{4} |HV\rangle \langle HV|$ , where  $|\tilde{\psi}\rangle = \frac{2}{\sqrt{6}} |HH\rangle + e^{-i\pi/4} \frac{1}{\sqrt{3}} |VV\rangle$ . One can see that  $\tau_{BD}^H$  is entangled. The same result is found if the measurement on  $C$  finds  $|V\rangle$ , and therefore the causal map is quantum in the common-cause pathway.

Finding  $B$  in the state  $|H\rangle$  also induces entanglement between  $C$  and  $D$ , as was already shown in the main text. For completeness, we note that, if one finds  $|V\rangle$  instead, the induced Choi state on  $CD$  is

$$\tau_{CD}^V = \frac{1}{2} |VV\rangle \langle VV| + \frac{1}{2} |\tilde{\varphi}\rangle \langle \tilde{\varphi}|, \quad (31)$$

with  $|\tilde{\varphi}\rangle \equiv \frac{1}{\sqrt{2}} (|HV\rangle + i|VH\rangle)$ , which is also entangled. As a result, the causal map  $\mathcal{E}_{CB|D}^{coh}$  satisfies all the requirements for the class COH: it is quantum in both the cause-effect and the common-cause pathways and, furthermore, exhibits a quantum Berkson effect.

*Example of PROBQ*

The circuit realizing an example of the class PROBQ is presented Fig. 4(c). This circuit implements a probabilistic mixture of identity and swap,

$$\begin{aligned} \mathcal{E}_{BF|DE}(\cdot) = & \frac{1}{2}(\mathbb{1}_{B|D} \otimes \mathbb{1}_{F|E})(\cdot) (\mathbb{1}_{B|D} \otimes \mathbb{1}_{F|E}) \\ & + \frac{1}{2}(\mathbb{1}_{B|E} \otimes \mathbb{1}_{F|D})(\cdot) (\mathbb{1}_{B|E} \otimes \mathbb{1}_{F|D}). \end{aligned} \quad (32)$$

Using supplementary equation 13, we find

$$\mathcal{E}_{CB|D}(\cdot) = \frac{1}{2}\mathcal{E}_{CB|D}^{ce}(\cdot) + \frac{1}{2}\mathcal{E}_{CB|D}^{cc}(\cdot), \quad (33)$$

where  $\mathcal{E}_{CB|D}^{ce}$  and  $\mathcal{E}_{CB|D}^{cc}$  are defined in supplementary equation 24 and supplementary equation 25 respectively. This shows explicitly that the map is a probabilistic mixture of a purely cause-effect term and a purely common-cause term.

By supplementary equation 14, the Choi state is

$$\tau_{CBD} = \frac{1}{2}\mathbb{1}_C \otimes |\Phi^+\rangle\langle\Phi^+|_{BD} + \frac{1}{2}|\Phi^+\rangle\langle\Phi^+|_{CB} \otimes \frac{1}{2}\mathbb{1}_D. \quad (34)$$

Finding  $C$  in the state  $|H\rangle$  implies  $\tau_{BD}^H = \frac{1}{2}|\Phi^+\rangle\langle\Phi^+|_{BD} + \frac{1}{2}|H\rangle\langle H|_B \otimes \frac{1}{2}\mathbb{1}_D$ , which is entangled, and similarly if  $C$  is found in the state  $|V\rangle$ . The causal map is therefore quantum in the cause-effect pathway. If we prepare  $|H\rangle$  on  $D$ , then the state on  $CB$  is  $\tau_{CB}^H = \frac{1}{2}|\Phi^+\rangle\langle\Phi^+|_{CB} + \frac{1}{2}(\frac{1}{2}\mathbb{1}_C \otimes |H\rangle\langle H|_B)$ , which is also entangled. The same holds when preparing  $|V\rangle$  on  $D$ , and consequently the causal map is quantum in the common-cause pathway. It follows that the causal map is in the class PROBQ.

*Causal maps that are classical on both pathways*

A general way to realize causal maps that are classical on both the cause-effect and common-cause pathway is to insert completely dephasing channels before and after the gate  $\mathcal{E}_{BF|DE}$ . The generic completely dephasing channel takes the form

$$\Delta_{\hat{n}}(\rho) = \frac{1}{2}\rho + \frac{1}{2}([\hat{n} \cdot \vec{\sigma}]\rho[\hat{n} \cdot \vec{\sigma}]), \quad (35)$$

where  $\vec{\sigma}$  is the vector of Pauli observables and the Bloch vector  $\hat{n}$  specifies the eigenbasis on which we dephase. The dephasing effectively reduces the qubits  $B, D, E$ , and  $F$  to classical binary variables, which we denote  $b, d, e, f$ , and reduces the map  $\mathcal{E}_{BF|DE}$  to a conditional probability distribution  $P(bf|de)$ : letting  $|b\rangle$  denote the elements of

a preferred basis of  $\mathcal{H}_B$  – namely, the eigenbasis of  $\hat{n}_B \cdot \vec{\sigma}$  –, and similarly for  $F, D$  and  $E$ , we can write

$$\begin{aligned} \mathcal{E}_{BF|DE}(\rho_{DE}) = & \sum_{b,d,e,f} P(bf|de) |b\rangle\langle b| \otimes |f\rangle\langle f| \\ & \times \text{Tr}_{DE}(|d\rangle\langle d| \otimes |e\rangle\langle e| \rho_{DE}). \end{aligned} \quad (36)$$

The dephasing on  $E$  also effectively reduces  $C$  to a classical binary variable, since  $C$  is only related to other variables in the problem via  $E$ . We denote this variable by  $c$  and the corresponding preferred basis (which generally depends on the initial joint state  $\rho_{CE}$ ) by  $|c\rangle$ . Substituting supplementary equation 36 into supplementary equation 13, we find that the causal map takes the form

$$\mathcal{E}_{CB|D}(\rho_D) \equiv \sum_{c,b,d} P(cb|d) |c\rangle\langle c| \otimes |b\rangle\langle b| \times \text{Tr}_D(|d\rangle\langle d| \rho_D). \quad (37)$$

Note that, since the prescription for deriving the causal map  $\mathcal{E}_{CB|D}$  from  $\mathcal{E}_{BF|DE}$  and  $\rho_{CE}$  involves tracing out system  $F$ , we find this form of the causal map independently of whether we actually apply dephasing on  $F$ : dephasing on  $D, E$  and  $B$  is sufficient.

It follows that the corresponding Choi state takes the form

$$\tau_{CBD} = \sum_{c,b,d} P(cb|d) u(d) |c\rangle\langle c| \otimes |b\rangle\langle b| \otimes |\tilde{d}\rangle\langle\tilde{d}|, \quad (38)$$

where  $u(d)$  denotes the uniform distribution over  $d$  and  $|\tilde{d}\rangle$  is related to  $|d\rangle$  by complex conjugation in the basis that defines the Choi isomorphism (in our case,  $\{|H\rangle, |V\rangle\}$ ). Similarly, the induced states, for a preparation  $\rho_D = |d\rangle\langle d|$ , projection  $\Pi_C^c = |c\rangle\langle c|$ , and projection  $\Pi_B^b = |b\rangle\langle b|$  are given by the operators

$$\begin{aligned} \tau_{CB}^d &= \sum_{c,b} P^d(c,b) |c\rangle\langle c| \otimes |b\rangle\langle b| \\ \tau_{BD}^c &= \sum_{b,d} P^c(b,d) |b\rangle\langle b| \otimes |\tilde{d}\rangle\langle\tilde{d}|, \\ \tau_{CD}^b &= \sum_{c,d} P^b(c,d) |c\rangle\langle c| \otimes |\tilde{d}\rangle\langle\tilde{d}|. \end{aligned} \quad (39)$$

with

$$\begin{aligned} P^d(c,b) &= P(cb|d) \\ P^c(b,d) &= P(cb|d)u(d) / \left[ \sum_{bd} P(cb|d)u(d) \right] \\ P^b(c,d) &= P(cb|d)u(d) / \left[ \sum_{cd} P(cb|d)u(d) \right]. \end{aligned} \quad (40)$$

Any operator of the form of supplementary equation 39 is separable. Therefore, by our criterion, such dephased causal maps are not quantum in either pathway.

*Example of PROBC*

A circuit realizing an example of PROBC is presented in Fig. 4(a). It applies complete dephasing channels to  $D$  and  $E$  only. However, note that  $B$  and  $F$  are obtained from  $D$  and  $E$  by either the two-qubit identity channel or the swap. This implies that  $B$  and  $F$  are also effectively classical, on the same bases on which we dephase  $D$  and  $E$ . The gate therefore can be expressed in the form of supplementary equation 36, with

$$P(bf|de) = \frac{1}{2}\delta_{b,d}\delta_{f,e} + \frac{1}{2}\delta_{b,e}\delta_{f,d}, \quad (41)$$

where  $\delta_{x,y}$  denotes the Kronecker delta function over variables  $x, y$ . The variables  $d$  and  $e$  are mapped either to  $b$  and  $f$  or to  $f$  and  $b$ , respectively, with equal probability: a probabilistic mixture of classical identity and swap. The causal map is therefore effectively described by a classical probability distribution, as in supplementary equation 37, with

$$P(cb|d) = \frac{1}{2}u(c)\delta_{b,d} + \frac{1}{2}\delta_{c,b}u(c), \quad (42)$$

where  $u(x)$  denotes the uniform distribution of the variable  $x$ . The dephasing ensures that the common-cause and cause-effect components of the causal map are classical, and the form of  $\mathcal{E}_{CB|D}$  makes it clear that this is a probabilistic mixture of classical cause-effect and common-cause relations. The causal map is therefore in the class PROBC.

*Example of PHYSC*

A circuit realizing an example of PHYSC is presented in Fig. 4(b). Again, we explicitly apply dephasing channels only to  $D$  and  $E$ , but note that the classical XNOR gate, which generates  $B$  in the left-hand panel, implicitly defines a preferred basis – in other words: if  $B$  is the output of a classical XNOR (Not-XOR:  $b = -de$  for  $d, e \in \{-1, 1\}$ ), then  $B$  must be (effectively) classical. In the right-hand panel,  $B$  is prepared in the maximally mixed state, which can also be described as effectively classical. The same holds for  $F$ , and we can therefore again express the causal map in terms of a classical conditional distribution,

$$P(bf|de) = \frac{1}{2}\delta_{b,-de}u(f) + \frac{1}{2}u(b)\delta_{f,-de}, \quad (43)$$

The gate either sets  $b = -de$  and generates  $f$  at random or vice versa. This leads to a causal map of the form of supplementary equation 37, with

$$P(cb|d) = \frac{1}{2}u(c)u(b) + \frac{1}{2}u(c)\delta_{b,-cd}. \quad (44)$$

Even though  $b$  is completely unaffected by  $d$  and  $e$  in the first term, in the second term  $b$  depends nontrivially on both inputs. One can see that this makes the causal map a physical mixture: indeed, the induced state  $\tau_{CD}^b$  in this case is given by supplementary equation 39 with

$$P^b(cd) = \frac{1}{2}u(c)u(d) + \frac{1}{2}u(c)\delta_{b,-cd}. \quad (45)$$

The mutual information between  $c$  and  $d$  in this distribution is 0.19 bits for either value of  $b$ . By contrast, we will show in a later section that the induced mutual information between binary variables  $c$  and  $d$  for any probabilistic mixture of common-cause and cause-effect with uniform prior distributions (which is the case here) is at most 0.12 bits. It follows that the present example must be a physical mixture, and noting furthermore that the causal map is classical in both pathways, we conclude that it belongs to the class PHYSC.

*Proof that COH is a strict subset of PHYSC*

Based on the previous scenarios, one can now see that COH is in fact a strict subset of PHYSC. To show this, we will explicitly construct a causal map that belongs to PHYSC but not to COH. To wit, consider a probabilistic mixture of our examples of PROBC and PHYSC, with a small weight  $\epsilon$  for the latter:

$$\begin{aligned} \mathcal{E}_{CB|D}(\cdot) &= \frac{1-\epsilon}{2} \left( \frac{1}{2}\mathbb{1}_C \otimes \mathcal{I}_{B|D}(\cdot) + |\Phi^+\rangle\langle\Phi^+|_{CB} \times \text{Tr}_D(\cdot) \right) \\ &+ \frac{\epsilon}{2} \left( \frac{1}{2}\mathbb{1}_C \otimes \frac{1}{2}\mathbb{1}_B \times \text{Tr}_D(\cdot) \right) \\ &+ \sum_{c,b,d} u(c)\delta_{b,-cd} |c\rangle\langle c| \otimes |b\rangle\langle b| \times \text{Tr}_D(|d\rangle\langle d| \cdot), \end{aligned} \quad (46)$$

where we take the preferred bases for the example of PHYSC,  $|c\rangle$ ,  $|b\rangle$  and  $|d\rangle$ , to each be the eigenbasis of  $\sigma_z$ .

In this case, the resulting causal map is still quantum on both pathways: indeed, finding  $C$  in the state  $|H\rangle$  implies

$$\begin{aligned} \tau_{BD}^H &= \frac{1-\epsilon}{2} |\Phi^+\rangle\langle\Phi^+|_{BD} + \frac{1-\epsilon}{2} |H\rangle\langle H|_B \otimes \frac{1}{2}\mathbb{1}_D \\ &+ \frac{\epsilon}{2} \frac{1}{2}\mathbb{1}_B \otimes \frac{1}{2}\mathbb{1}_D + \frac{\epsilon}{2} \sum_{b,d} u(d)\delta_{b,-d} |b\rangle\langle b| \otimes |\tilde{d}\rangle\langle\tilde{d}|, \end{aligned} \quad (47)$$

which is entangled for a range of  $\epsilon$ , and similarly for finding  $C$  in the state  $|V\rangle$ . The causal map is therefore quantum in the cause-effect pathway. If we prepare  $|H\rangle$  on  $D$ , then the state on  $CB$  is

$$\begin{aligned} \tau_{CB}^H &= \frac{1-\epsilon}{2} |\Phi^+\rangle\langle\Phi^+|_{CB} + \frac{1-\epsilon}{2} \frac{1}{2}\mathbb{1}_C \otimes |H\rangle\langle H|_B \\ &+ \frac{\epsilon}{2} \frac{1}{2}\mathbb{1}_C \otimes \frac{1}{2}\mathbb{1}_B + \frac{\epsilon}{2} \sum_{c,b} u(c)\delta_{b,-c} |c\rangle\langle c| \otimes |b\rangle\langle b|, \end{aligned} \quad (48)$$



which is also entangled. The same holds for preparing  $|V\rangle$  on  $D$ , and consequently the causal map is quantum in the common-cause pathway. However, the causal map cannot be realized by a probabilistic mixture of purely common-cause and purely cause-effect relations, since the witness of physical mixture is  $\epsilon/4$ , i.e. non-zero for all valid values of  $\epsilon$ . (The fact that the last term,  $b = -cd$ , has  $b$  depending simultaneously on  $c$  and  $d$  is also suggestive of a physical mixture, but not conclusive.) Consequently, the map belongs to PHYSQ.

On the other hand, no measurement outcome on  $B$  implies entanglement on  $CD$ : since every term in the expression for  $\mathcal{E}_{CB|D}$  has the form of a tensor product between  $C$  and  $D$ , the state induced when selecting for any state on  $B$  must be separable. It follows that the map is not in COH.

### Supplementary Note 3: Implementing the examples using a single experimental set-up

In the following section, we show how the single set-up in Fig. 5 can experimentally realize our examples of the classes COH (hence PHYSQ), PROBQ, PROBC, and PHYSC. We first describe the implementation of the partial swap gate, which allows us to realize the example of COH from Fig. 4(d). Next we describe how this gate can be modified in order to realize the example of PROBQ from Fig. 4(c). We then move on to discuss how applying complete dephasing channels on  $D$ ,  $E$  and  $B$  yields causal maps where both pathways are classical. We show that by modifying the type of dephasing, we can realize the examples of PROBC and PHYSC (up to a sign change) presented in Fig. 4(a,b).

#### Example of COH

We begin by describing how the partial swap gate is implemented experimentally. In the set-up of Fig. 5, two photons are input at  $D$  and  $E$  and measured in coincidence at  $B$  and  $F$ . If the photons input at  $D$  and  $E$  are indistinguishable, then when they arrive at the first beam splitter, they will bunch if their polarization state lies in the symmetric subspace (spanned by the triplet basis), while they will anti-bunch if their polarization state lies in the anti-symmetric subspace (singlet). If they bunch, then a coincidence at  $B$  and  $F$  can only be obtained if both photons take the clockwise path in the Sagnac interferometer. However, if they anti-bunch, the two photons will take opposite paths. The photon travelling along counterclockwise path will acquire an extra phase, denoted  $\theta$ , due to the glass windows, while the other, on the clockwise path, acquires no extra phase.

In this configuration, the gate applies a phase difference between the symmetric and anti-symmetric subspaces of the photon state. Recall that the projectors onto these subspaces can be written as linear combinations of the identity and swap operators,

$$\begin{aligned}\mathbb{S} &= \frac{1}{2} (\mathbb{1}_{B|D} \otimes \mathbb{1}_{F|E} + \mathbb{1}_{B|E} \otimes \mathbb{1}_{F|D}) \\ \mathbb{A} &= \frac{1}{2} (\mathbb{1}_{B|D} \otimes \mathbb{1}_{F|E} - \mathbb{1}_{B|E} \otimes \mathbb{1}_{F|D}),\end{aligned}\quad (49)$$

so that the gate takes the form

$$\mathcal{E}_{BF|DE}(\rho) = (\mathbb{S} + e^{i\theta}\mathbb{A})\rho(\mathbb{S} + e^{i\theta}\mathbb{A})^\dagger. \quad (50)$$

Substituting the expressions for  $\mathbb{S}$  and  $\mathbb{A}$ , we find

$$\begin{aligned}\mathbb{S} + e^{i\theta}\mathbb{A} &= \\ &= \frac{\mathbb{1}_{B|D} \otimes \mathbb{1}_{F|E} + \mathbb{1}_{B|E} \otimes \mathbb{1}_{F|D}}{2} \\ &\quad + e^{i\theta} \frac{\mathbb{1}_{B|D} \otimes \mathbb{1}_{F|E} - \mathbb{1}_{B|E} \otimes \mathbb{1}_{F|D}}{2} \\ &= e^{i\theta/2} (\cos(\theta/2)\mathbb{1}_{B|D} \otimes \mathbb{1}_{F|E} - i \sin(\theta/2)\mathbb{1}_{B|E} \otimes \mathbb{1}_{F|D})\end{aligned}\quad (51)$$

Thus, by adjusting the phase of the Sagnac interferometer to  $\theta = -\pi/2$ , we obtain a gate  $\mathcal{E}_{BF|DE}$  that implements the partial swap unitary  $U_{BF|DE}$  given by equation 2 in the main text. This allows us to build the circuit in Fig. 4(d) and realize our example of the class COH.

#### Example of PROBQ

In order to realize our example of the class PROBQ, we modify the experimental set-up as follows. If we delay photon  $E$  with respect to photon  $D$ , which can be accomplished using a translation stage, then the two-photon interference at the beam splitter no longer occurs. The two pathways that lead to a coincidence measurement at  $B$  and  $F$  remain the same, but they no longer act coherently. The gate can instead be understood to project into the symmetric and anti-symmetric subspaces: in terms of the operators  $\mathbb{S}$  and  $\mathbb{A}$  defined in supplementary equation 49,

$$\mathcal{E}_{BF|DE}(\cdot) = \mathbb{S}(\cdot)\mathbb{S} + \mathbb{A}(\cdot)\mathbb{A}. \quad (52)$$

Substituting the expressions from supplementary equation 49, we find that this expression is equivalent to the probabilistic mixture of identity and swap of supplementary equation 32:

$$\begin{aligned}\mathcal{E}_{BF|DE}(\cdot) &= \frac{1}{2}(\mathbb{1}_{B|D} \otimes \mathbb{1}_{F|E}) (\cdot) (\mathbb{1}_{B|D} \otimes \mathbb{1}_{F|E}) \\ &\quad + \frac{1}{2}(\mathbb{1}_{B|E} \otimes \mathbb{1}_{F|D}) (\cdot) (\mathbb{1}_{B|E} \otimes \mathbb{1}_{F|D}).\end{aligned}\quad (53)$$

We note that, unlike the previous case, the overall gate does not depend on the relative phase  $\theta$  of the clockwise and anti-clockwise paths through the Sagnac interferometer. Here, the beam splitter reflectivity adjusts the relative weights of identity and swap. For a 50-50 beam splitter, as used in the experiment, both the identity and swap operations will have equal weights and we obtain the circuit of Fig. 4(c), which implements an example of the class PROBC.

#### Example of PROBC

In order to experimentally realize our example of the class PROBC, we modify the gate  $\mathcal{E}_{BF|DE}$  from supplementary equation 50 by applying complete dephasing along the  $\hat{z}$  axis to  $E$ ,  $D$ , and  $B$ , so that

$$\mathcal{E}_{BF|DE}(\cdot) = (\Delta_z^B \otimes \mathcal{I}_F) \left( U_{BF|DE} \left( (\Delta_z^D \otimes \Delta_z^E)(\cdot) \right) U_{BF|DE}^\dagger \right). \quad (54)$$

Using supplementary equation 13, the causal map is found to be

$$\mathcal{E}_{CB|D}(\cdot) = \frac{1}{2} \mathbb{1}_C \otimes \Delta_z^B \circ \mathcal{I}_{B|D}(\cdot) + \frac{1}{2} (\Delta_z^C \otimes \Delta_z^B) (|\Phi^+\rangle\langle\Phi^+|_{CB}) \text{Tr}_D(\cdot). \quad (55)$$

One can see that this causal map takes the effectively classical form of supplementary equation 37, with  $|c\rangle$ ,  $|b\rangle$  and  $|d\rangle$  all denoting eigenstates of  $\sigma_z$ , and

$$P(cb|d) = \frac{1}{2} u(c) \delta_{b,d} + \frac{1}{2} \delta_{c,b} u(c), \quad (56)$$

which is exactly the same as in our example of Fig. 4(a). As we pointed out in the previous discussion of this example (around supplementary equation 42), the causal map is classical in both pathways (due to the dephasing) and manifestly takes the form of a probabilistic mixture, hence it belongs to PROBC.

#### Example of PHYSC

The class PHYSC is experimentally realized by applying complete dephasing in the eigenbases of  $\sigma_x$  on  $E$ ,  $\sigma_y$  on  $D$  and  $\sigma_z$  on  $B$ . This choice of bases ensures that the witness of physical mixture, which is evaluated using only measurements of these particular observables, remains unchanged by the dephasing. It therefore ensures that we continue to realize a physical mixture while eliminating the coherence in the cause-effect and common-cause paths. Combining the dephasing channels with the partial swap unitary, we can write the overall two-qubit gate

in this scenario as

$$\mathcal{E}_{BF|DE}(\cdot) = (\Delta_z^B \otimes \mathcal{I}_F) \left( U_{BF|DE} \left( (\Delta_y^D \otimes \Delta_x^E)(\cdot) \right) U_{BF|DE}^\dagger \right). \quad (57)$$

Since the dephasing introduces a different preferred basis for each of the qubits, we will use the notation  $|c_x\rangle$ ,  $|d_y\rangle$  and  $|b_z\rangle$ , with  $\{c, d, b\} \in \pm 1$ , for the eigenstates of the Pauli operators  $\sigma_x$ ,  $\sigma_y$  and  $\sigma_z$ , respectively. Inserting  $\mathcal{E}_{BF|DE}$  into supplementary equation 13, one can obtain the causal map  $\mathcal{E}_{CB|D}$ , which takes the special form shown in supplementary equation 37 with  $P(cb|d)$  given by supplementary equation 44. Similarly, the corresponding Choi state is diagonal in the bases  $|\pm_x\rangle$  on  $C$ ,  $|\pm_z\rangle$  on  $B$  and  $|\pm_y\rangle$  on  $D$ :

$$\begin{aligned} \tau_{CBD} = & \frac{1}{16} \mathbb{1}_{CBD} \\ & + \frac{1}{8} |+_x\rangle\langle+_x|_C \otimes |-_z\rangle\langle-_z|_B \otimes |-_y\rangle\langle-_y|_D \\ & + \frac{1}{8} |-_x\rangle\langle-_x|_C \otimes |-_z\rangle\langle-_z|_B \otimes |+_y\rangle\langle+_y|_D \\ & + \frac{1}{8} |+_x\rangle\langle+_x|_C \otimes |+_z\rangle\langle+_z|_B \otimes |+_y\rangle\langle+_y|_D \\ & + \frac{1}{8} |-_x\rangle\langle-_x|_C \otimes |+_z\rangle\langle+_z|_B \otimes |-_y\rangle\langle-_y|_D \end{aligned} \quad (58)$$

(As pointed out after supplementary equation 38, the basis  $|d\rangle$  that diagonalizes the Choi state is related to the basis  $|d\rangle$  that diagonalizes the causal map by complex conjugation in the basis that defines the Choi isomorphism. In our case,  $|d\rangle$  are eigenstates of  $\sigma_y$ , and the Choi isomorphism is defined by the eigenbasis of  $\sigma_z$ , hence  $|\tilde{d}\rangle$  are also eigenstates of  $\sigma_y$ , albeit with the opposite eigenvalues.)

Since the output  $B$  depends on whether  $C$  and  $D$  are correlated or anti-correlated, the causal structure cannot be described by a probabilistic mixture of purely cause-effect and purely common-cause mechanisms. Indeed, one can see that the causal map is effectively classical, since it takes the form of supplementary equation 37, and the classical conditional distribution  $P(cb|d)$  has the same form as supplementary equation 44 (up to an exchange of positive and negative correlations). Since both pathways of the causal map are classical, we conclude that it belongs to PHYSC.

#### Supplementary Note 4: Reconstructing the causal map and obtaining the negativity from experimental data

This section details how we reconstruct causal maps from experimental data using a maximum likelihood estimation. The analysis is based on [9].

The measurement statistics obtained in the experiment take the form of count numbers for different combinations of wave plate orientations. We measure the Pauli observable  $\sigma_s$  on  $C$  and  $\sigma_u$  on  $B$ , denoting the resulting eigenvalues by  $c$  and  $b$ , respectively, and prepare the  $d$

eigenstate of  $\sigma_t$  on  $D$ , where  $s, t, u \in \{1, 2, 3\}$  range over  $\sigma_1 \equiv \sigma_x$ ,  $\sigma_2 \equiv \sigma_y$  and  $\sigma_3 \equiv \sigma_z$ . Since the orientation of the wave plates encodes both the choice of observable and the selected eigenstate, the outcome in this case is not one of two possible eigenvalues, but rather whether the photon reaches the detector in the end, indicating that it was in the desired eigenstate. The observed count numbers for the wave plate orientations specified by  $cbdstu$  are denoted  $\tilde{P}^{\text{obs}}(cbdstu)$ . The expected count numbers for wave plate orientations encoding  $s, c, t, d$  and  $u, b$  are therefore proportional to the joint probabilities of realizing the eigenvalues  $c, b, d$  and the choices of Pauli operators  $s, t, u$ . We denote the expected count numbers predicted by the fitting model by

$$\tilde{P}^{\text{fit}}(cbdstu) = NP^{\text{fit}}(cbdstu), \quad (59)$$

where  $P^{\text{fit}}(cbdstu)$  is the joint probability distribution predicted by the fitting model and  $N$  is the number of runs of the experiment.

Let us now relate the joint probability distribution  $P^{\text{fit}}(cbdstu)$  to the model parameters, in particular the Choi state  $\tau_{CBD}$  which represents the causal map. To this end, we introduce the notation  $\Pi_C^{s,c}$  for the projector onto the  $c \in \{\pm 1\}$  eigenstate of the Pauli operator  $\sigma_s$ , with  $s \in \{1, 2, 3\}$ . The conditional probability of finding eigenvalues  $c, b$ , given that one chose Pauli observables  $s, t, u$  and prepared the  $d$  eigenstate on  $D$ , can then be written in terms of the causal map and its Choi state as

$$\begin{aligned} P^{\text{fit}}(cb|dstu) &\equiv \text{Tr} \left[ \Pi_C^{s,c} \otimes \Pi_B^{u,b} \mathcal{E}_{CB|D} \left( \Pi_D^{t,d} \right) \right] \\ &\equiv 2\text{Tr} \left[ T_D (\tau_{CBD}) \Pi_C^{s,c} \otimes \Pi_B^{u,b} \otimes \Pi_D^{t,d} \right], \end{aligned} \quad (60)$$

where  $T_D$  denotes the transpose with respect to the input system  $D$ . In our experiment, we choose which eigenstate  $d$  to prepare by rotating the wave plates after the polarizing beam-splitter, with each setting being implemented for an equal period of time. Under the assumptions of a constant rate of photon production (on average) and equal transmission efficiency of the wave plates with different settings, this can be modelled by simply taking the probability of each eigenvalue to be  $P(d|t) = \frac{1}{2}$  for  $d = \pm 1$ ,  $t = 1, 2, 3$ . In this case, the probabilities of eigenvalues  $c, b, d$  given the settings (choices of eigenbasis)  $s, t, u$  become

$$\begin{aligned} P^{\text{fit}}(cbd|stu) &= P^{\text{fit}}(cb|dstu)P^{\text{fit}}(d|t) \\ &= \text{Tr} \left[ \tau_{CBD} \cdot \Pi_C^{s,c} \otimes \Pi_B^{u,b} \otimes T_D \left( \Pi_D^{t,d} \right) \right], \end{aligned} \quad (61)$$

where we note that the probability of outcome  $d$  in the measurement on  $D$  is independent of the settings of the other two measurements, that is,  $P(d|stu) = P(d|t)$ . Finally, we note that the choice of observables  $s, t, u$  in our experiment is made at random, so that

$P(stu) = \frac{1}{27}$  for all values of  $s, t, u$ . Using the chain rule  $P(cbdstu) = P(cbd|stu)P(stu)$ , we can finally write the expected count numbers in terms of the model parameters:

$$\tilde{P}^{\text{fit}}(cbdstu) = \text{Tr} \left[ \frac{N}{27} \tau_{CBD} \cdot \Pi_C^{s,c} \otimes \Pi_B^{u,b} \otimes T_D \left( \Pi_D^{t,d} \right) \right]. \quad (62)$$

The operator  $\tau_{CBD}$  that parametrizes the model is subject to certain consistency constraints: as a Choi state, it must be positive semi-definite and have trace one, while the combination  $\frac{N}{27}\tau_{CBD}$  need only be positive, but not normalized. Following Ref. [30], this is achieved with the following parameterization:

$$\tau_{CBD} = \frac{N}{27} J_{CBD}^\dagger J_{CBD}, \quad (63)$$

where  $J_{CBD}$  is an 8x8 lower triangular matrix with real diagonal elements, specified by 64 real parameters. This form, known as the Cholesky decomposition, is positive-semidefinite by design, and, by varying over  $J_{CBD}$ , ranges over all positive operators. We normalize to trace one after the optimization by dividing by  $\text{Tr}(J_{CBD}^\dagger J_{CBD})$ .

A second constraint arises due to the particular configuration of our experimental setup: since the preparation  $D$  occurs after the measurement of  $C$ , the input at  $D$  cannot have any causal influence on the measurement outcome at  $C$ . Therefore, the marginal  $\tau_{CD} \equiv \text{Tr}_B(\tau_{CBD})$  must be independent of  $D$ ,

$$\tau_{CD} = \rho_C \otimes \frac{1}{2}, \quad (64)$$

where  $\rho_C = \text{Tr}_{BD}(\tau_{CBD})$ .

We include this additional constraint in the least-squares fit by adding penalty functions to the residue, so that the overall argument becomes

$$\begin{aligned} \chi^2 &= \sum_{cbdstu} \frac{\left[ \tilde{P}^{\text{obs}}(cbdstu) - \tilde{P}^{\text{fit}}(cbdstu) \right]^2}{\tilde{P}^{\text{fit}}(cbdstu)} \\ &\quad + \lambda \sum_{ij} \left| \left( \tau_{CD} - \rho_C \otimes \frac{1}{2} \right)_{ij} \right|^2. \end{aligned} \quad (65)$$

To enforce these constraints but not overshadow the principal function, the value of the Lagrange multiplier,  $\lambda$  was selected heuristically to be  $10^7$ .

#### Obtaining the negativity from experimental data

We now describe how to obtain the negativity of the induced states  $\tau_{CB}^d$ ,  $\tau_{BD}^c$ , and  $\tau_{CD}^b$  from experimental data. Since the method is similar for all three, we will only illustrate it for the last case. In order to measure

entanglement in  $\tau_{CD}^b$ , we first reconstruct the state as a 2-qubit operator on  $C$  and  $D$ , using only count numbers from runs in which we found a particular eigenstate  $\Pi^{u,b}$  on  $B$ , denoted  $\tilde{P}^{\text{obs}}(cdst|bu)$ . Following the model from the least-squares reconstruction of the full causal map, and still assuming that the preparations on  $D$  can be modelled with  $P(d) = \frac{1}{2}$ , the joint count numbers take the form of supplementary equation 62. We post-select on an outcome  $b$ , assuming the measurement basis  $u$  to be fixed. This gives rise to the conditional distribution

$$\begin{aligned} \tilde{P}^{\text{fit}}(cdst|bu) &= \\ &= \frac{N}{9} \text{Tr}_{CD} \left[ \frac{1}{P(b|u)} \text{Tr}_B \left( \Pi_B^{u,b} \tau_{CBD} \right) \Pi_C^{s,c} \otimes T_D \left( \Pi_D^{t,d} \right) \right] \\ &= \frac{N}{9} \text{Tr}_{CD} \left[ \tau_{CD}^b \Pi_C^{s,c} \otimes T_D \left( \Pi_D^{t,d} \right) \right]. \end{aligned} \quad (66)$$

Although a full specification of the state on  $B$  on which we post-select specifies both the eigenvalue  $b$  and the choice of observable  $u$ , since the latter is assumed fixed, we suppress it and write simply  $\tau_{CD}^b$ . The model against which we compare the observed count numbers can therefore be written as

$$\tilde{P}^{\text{fit}}(cdst|b) = \text{Tr}_{CD} \left[ \frac{N}{9} \tau_{CD}^b \Pi_C^{s,c} \otimes T_D \left( \Pi_D^{t,d} \right) \right]. \quad (67)$$

The reconstruction method is then essentially the same as for the full causal maps: we parametrize  $\tau_{CD}^b$  as a 4x4 lower triangular matrix with 16 real parameters and minimize the residue

$$\chi^2 = \sum_{cdst} \frac{\left[ \tilde{P}^{\text{obs}}(cdst) - \tilde{P}^{\text{fit}}(cdst) \right]^2}{\tilde{P}^{\text{fit}}(cdst)}. \quad (68)$$

Once the optimal parameters have been found, the negativity,  $\mathcal{N}$ , of the reconstructed state  $\tau_{CD}^b$  is calculated using equation 5. Negativities for the induced states  $\tau_{CB}^d$  and  $\tau_{BD}^c$  are calculated in a similar way.

### Supplementary Note 5: Witness of physical mixture

In this section, we define a family of functions of the experimental statistics that witness physical mixtures of common-cause and cause-effect mechanisms. In other words, we seek functions that are zero for all probabilistic mixtures and non-zero for at least some physical mixtures. For simplicity, we restrict ourselves to the case of qubits.

The witness is defined in terms of the statistics of measurements of a single Pauli observable on each  $C$  and  $B$  and preparations of eigenstates of a third Pauli observable on  $D$ . That is, the settings  $s, t, u$  are fixed, with each choice giving rise to a different witness from the same family, and we omit them in the following for brevity.

When calculating the witness, we choose the eigenvalue  $d$  for the preparation of  $D$  from the uniform distribution,  $P(d) = \frac{1}{2}$  for  $d = \pm 1$ , and hence the joint probability distribution  $P(cdb)$  takes the same form as in supplementary equation 61.

### Properties of probabilistic mixtures

We begin by noting several mathematical properties of probabilistic mixtures that will be useful in the subsequent derivations.

As already shown, the Choi state representing a causal map that is a probabilistic mixture of common-cause and cause-effect can always be expressed as a sum of only two terms,

$$\tau_{CBD}^{\text{prob}} = p\rho_{CB} \otimes \frac{1}{2}\mathbb{1}_D + (1-p)\rho_C \otimes \tau_{BD}. \quad (69)$$

The first term represents the common-cause scenario, wherein we prepare a bipartite state  $\rho_{CB}$  and trace out  $D$ ; hence the marginal on  $D$  of the Choi state is the completely mixed state. The state  $\rho_{CB}$  is obtained from the initial state  $\rho_{CE}$  by a CPTP map that takes  $E$  to  $B$ , hence the marginal on  $C$  is unchanged:  $\text{Tr}_B \rho_{CB} = \text{Tr}_E \rho_{CE}$ . The second term corresponds to a cause-effect scenario, in which case the marginal state on  $C$  is simply the marginal of the initial bipartite state  $\rho_{CE}$ ,  $\rho_C = \text{Tr}_E \rho_{CE}$ . Meanwhile,  $\tau_{BD}$  is the Choi state corresponding to a CPTP map from  $D$  to  $B$ , hence its marginal on  $D$  is again the completely mixed state. In summary, the marginals of the two terms on  $C$  and  $D$ , respectively, are equal:

$$\text{Tr}_B \rho_{CB} = \text{Tr}_E \rho_{CE} = \rho_C, \quad (70)$$

$$\text{Tr}_B \tau_{BD} = \frac{1}{2}\mathbb{1}_D. \quad (71)$$

It furthermore holds for all causal maps that  $C$  and  $D$  become independent if we ignore  $B$ :

$$\text{Tr}_B [\tau_{CBD}] = \rho_C \otimes \frac{1}{2}\mathbb{1}_D. \quad (72)$$

The experimental statistics inherit these properties: letting  $u(d) \equiv \frac{1}{2} \forall d = \pm 1$  denote the uniform probability distribution, we have

$$P(cdb) = pP_{CB}(cb)u(d) + (1-p)P_C(c)P_{BD}(bd). \quad (73)$$

The marginal distributions over  $c$  and  $d$  in both terms are identical,

$$\sum_b P_{CB}(cb) = P_C(c), \quad (74)$$

$$\sum_b P_{BD}(bd) = u(d), \quad (75)$$

and, if we ignore  $b$ , then  $c$  and  $d$  become independent,

$$\sum_b P(cdb) = P_C(c)u(d). \quad (76)$$

*Simplification in limiting case*

*Intuitive simple version of the witness*

Suppose that the marginal on  $C$  is completely mixed, so that a probabilistic mixture of common-cause and cause-effect takes the form

$$\tau'_{CBD} = p\rho_{CB} \otimes \frac{1}{2}\mathbb{1}_D + (1-p)\frac{1}{2}\mathbb{1}_C \otimes \tau_{BD}, \quad (77)$$

with

$$\text{Tr}_B \rho_{CB} = \frac{1}{2}\mathbb{1}_C, \quad \text{Tr}_B \tau_{BD} = \frac{1}{2}\mathbb{1}_D. \quad (78)$$

Under this assumption, we can construct a witness in terms of the joint probabilities of supplementary equation 61 which is simply the expectation value of  $\tau_{CBD}$  for a product of Pauli observables,

$$\begin{aligned} \mathcal{C}_{CD}^0 &\equiv \sum_{cdb} cdb P(cdb) \\ &= \text{Tr} [\tau_{CBD} \sigma_C^s \otimes \sigma_B^u \otimes T_D(\sigma_D^t)], \end{aligned} \quad (79)$$

For any  $s, t, u \in 1, 2, 3$ , this is zero for any probabilistic mixture, as can be seen by inserting supplementary equation 77 into supplementary equation 79. Therefore, if one can assume that  $\rho_C = \frac{1}{2}\mathbb{1}$ , then non-zero value of  $\mathcal{C}_{CD}^0$  heralds a physical mixture.

*General form of the witness*

If we cannot justify the assumption that  $\rho_C = \frac{1}{2}\mathbb{1}$ , then we must use a more general version of the witness. We will now propose such a witness: a measure of induced correlations that is designed to be zero for probabilistic mixtures even if  $\rho_C \neq \frac{1}{2}\mathbb{1}$ .

Given the joint distribution  $P(cbd)$ , one can calculate the marginal  $P(b) = \sum_{cd} P(cbd)$  and the conditional distribution  $P(cd|b) = P(cbd)/P(b)$ . For each value of  $b$ , the latter is a distribution over  $c$  and  $d$ , and therefore the correlations between the two can be quantified by their covariance,

$$\begin{aligned} \text{cov}(c, d|b) &= \sum_{cd} cd P(cd|b) \\ &\quad - \left[ \sum_{cd} c P(cd|b) \right] \left[ \sum_{cd} d P(cd|b) \right]. \end{aligned} \quad (80)$$

We now define our witness to be the weighted difference of the covariances in the conditional distributions,

$$\mathcal{C}_{CD} = 2 \sum_{b=\pm 1} b P(b)^2 \text{cov}(cd|b). \quad (81)$$

We will prove that this choice has the desired properties in the following.

The witness  $\mathcal{C}_{CD}$  reduces to  $\mathcal{C}_{CD}^0$  if certain marginals of  $P(cdb)$  are uniform, specifically, if

$$P(cb) \equiv \sum_d P(cdb) = \frac{1}{4} \quad \forall c, b, \quad (82)$$

$$P(db) \equiv \sum_c P(cdb) = \frac{1}{4} \quad \forall d, b. \quad (83)$$

This ensures that each  $b$  occurs with equal probability,  $P(b) = \frac{1}{2}$ , and consequently the conditional distributions also satisfy

$$P(c|b) \equiv \sum_d P(cd|b) = \frac{1}{2} \quad \forall c, b, \quad (84)$$

$$P(d|b) \equiv \sum_c P(cd|b) = \frac{1}{2} \quad \forall d, b, \quad (85)$$

that is, the conditional distribution  $P(cd|b)$  has uniform marginals on  $c$  and  $d$ . The expectation values  $\langle c \rangle$  and  $\langle d \rangle$  under this distribution are zero, so that the covariance simplifies to

$$\text{cov}(c, d|b) = \langle cd \rangle = \sum_{cd} cd P(cd|b), \quad (86)$$

and therefore

$$\begin{aligned} \mathcal{C}_{CD} &= 2 \sum_b b P(b)^2 \sum_{cd} cd P(cd|b) \\ &= \sum_{cdb} cdb P(cdb) \equiv \mathcal{C}_{CD}^0. \end{aligned} \quad (87)$$

In this sense, the witness  $\mathcal{C}_{CD}$  is a generalization of the expectation value of the simple product of Paulis that defines  $\mathcal{C}_{CD}^0$

*Casting  $\mathcal{C}_{CD} = 0$  directly in terms of count numbers*

In order to facilitate the proof below as well as the assessment of whether or not  $\mathcal{C}_{CD} = 0$  based on experimental data, we cast the witness in a different form. To this end, we note that, if  $c$  and  $d$  are binary variables whose values are labelled  $\pm 1$ , then their covariance under a conditional distribution  $P(cd|b)$  takes the form

$$\text{cov}(c, d|b) = 4 [P(++|b)P(--|b) - P(+-|b)P(-+|b)]. \quad (88)$$

This allows us to rewrite the witness in terms of the joint probabilities  $P(cbd)$  as

$$\mathcal{C}_{CD} \equiv 8 \sum_{b=\pm 1} b [P(++|b)P(--|b) - P(+-|b)P(-+|b)]. \quad (89)$$

$\mathcal{C}_{CD} = 0$  for probabilistic mixtures

Now we can show that  $\mathcal{C}_{CD}$  is zero for any probabilistic mixture of common-cause and cause-effect relations. Recall that, since  $b$  only takes two values, the marginal independence (supplementary equation 76),

$$\sum_b P(cdb) = P_C(c)u(d) = \frac{1}{2}P_C(c) \quad (90)$$

implies that

$$P(cd, -) = \frac{P_C(c)}{2} - P(cd, +). \quad (91)$$

This allows us to rewrite the  $b = -1$  term in supplementary equation 89 as

$$\begin{aligned} & P(++,-)P(--,-) - P(+,-,-)P(-+,-) \\ &= -\frac{P_C(+)}{2}P(--,+)-\frac{P_C(-)}{2}P(++,+), \\ &+ \frac{P_C(+)}{2}P(-+,+)+\frac{P_C(-)}{2}P(+-,+) \\ &+ [P(++,+)-P(--,+)-P(+-,+)-P(-+,+)], \end{aligned} \quad (92)$$

hence the witness reduces to

$$\mathcal{C}_{CD} = 4[P_C(-)P(++,+)-P_C(-)P(+-,+)-P_C(+)-P(-+,+)+P_C(+)-P(--,+)] \quad (93)$$

$$= 4 \sum_{cd} cd [1 - P_C(c)] P(cd, +) \quad (94)$$

Our core hypothesis, of a probabilistic mixture, implies that  $P(cd, +)$  is a convex combination of two terms, each one a product distribution over  $cd$ . Substituting supplementary equation 73 and distributing the sums,

$$\begin{aligned} \mathcal{C}_{CD} = & 4p \left[ \sum_c c [1 - P_C(c)] P_{CB}(c, +) \right] \left[ \sum_d d u(d) \right] \\ & + 4(1-p) \left[ \sum_c c [1 - P_C(c)] P_C(c) \right] \left[ \sum_d P_{BD}(d, +) \right]. \end{aligned} \quad (95)$$

In the first term, we have the average over  $d = \pm 1$  under the uniform distribution, which is zero. In the second term, the sum over  $c$  gives  $P_C(+)-P_C(-)-P_C(-)-P_C(+)=0$ . Thus, for any causal map that is a probabilistic mixture of cause-effect and common-cause mechanisms of the form of supplementary equation 69, we have

$$\mathcal{C}_{CD} = 0. \quad (96)$$

We calculate the witness  $\mathcal{C}_{CD}$  explicitly from experimental count numbers  $\tilde{P}(c, d, b)$  using supplementary equation 89,

$$\mathcal{C}_{CD} = \frac{\sum_{b=\pm 1} b \left( \tilde{P}(++b)\tilde{P}(- - b) - \tilde{P}(+-b)\tilde{P}(- + b) \right)}{\left( \sum_{c,d,b=\pm 1} \tilde{P}(c, d, b) \right)^2}. \quad (97)$$

The uncertainty on the witness is calculated by assuming Poissonian noise on the count numbers and propagating the errors through supplementary equation 97.

### Supplementary Note 6: Bounds on induced mutual information in Berkson's paradox

In the following, we derive an upper bound on the mutual information between two causes,  $D$  and  $E$ , conditioned on their common effect,  $B$ , under the assumption that the two influences are combined probabilistically, that is,

$$P(B|DE) = (1-p)P_{\mathcal{D}}(B|D) + pP_{\mathcal{E}}(B|E). \quad (98)$$

The derivation is cast in terms of classical variables, but an extension to the quantum case is given at the end.

The distribution over  $DE$  conditional on some value of  $B$  can be obtained by Bayesian inversion. Note that, since  $D$  and  $E$  do not share a common cause, our prior probability distribution over them takes the form of a product of two generic probability distributions, which we denote by  $Q(D)$  and  $Q(E)$ . It follows that

$$\begin{aligned} P(DE|B) &\equiv P(B|DE)P(DE)/P(B) \\ &= (1-p)Q(E)\frac{P_{\mathcal{D}}(B|D)Q(D)}{P(B)} \\ &+ pQ(D)\frac{P_{\mathcal{E}}(B|E)Q(E)}{P(B)}, \end{aligned} \quad (99)$$

where  $P(B) \equiv \sum_{DE} P(B|DE)Q(D)Q(E)$ . For each value  $b$  of  $B$ , the fractions are distributions over  $D$  and  $E$ , respectively, but not necessarily normalized. Let  $P_{\mathcal{D}}^b(D)$  and  $P_{\mathcal{E}}^b(E)$  denote the corresponding normalized distributions, introducing the  $b$ -dependent modified weight  $q^b$  to absorb the difference in normalization:

$$q^b = p \frac{1}{P(B=b)} \sum_E P_{\mathcal{E}}(B=b|E)Q(E), \quad (100)$$

or, equivalently,

$$(1-q^b) = (1-p) \frac{1}{P(B=b)} \sum_D P_{\mathcal{D}}(B=b|D)Q(D), \quad (101)$$

and

$$P_{\mathcal{E}}^b(E) = \frac{p}{q^b} \frac{1}{P(B=b)} P_{\mathcal{E}}(B=b|E)Q(E) \quad (102)$$

$$P_{\mathcal{D}}^b(D) = \frac{1-p}{1-q^b} \frac{1}{P(B=b)} P_{\mathcal{D}}(B=b|D)Q(D). \quad (103)$$

For the purpose of this derivation, we will focus on a single value  $b$  and, for brevity, suppress the explicit  $b$ -dependence in the following. In this new notation,

$$P(DE) = (1-q)Q(E)P_{\mathcal{D}}(D) + qQ(D)P_{\mathcal{E}}(E). \quad (104)$$

We will show that the mutual information  $I(D : E)$  in this distribution is maximal if  $P_{\mathcal{D}}(D)$  and  $P_{\mathcal{E}}(E)$  each produce a single value with certainty. To see this, consider the mutual information as a functional of two arguments, the marginal distribution over  $E$ ,

$$P(E) = (1-q)Q(E) + qP_{\mathcal{E}}(E), \quad (105)$$

and the conditional

$$P(D|E) = \frac{(1-q)Q(E)}{(1-q)Q(E) + qP_{\mathcal{E}}(E)} P_{\mathcal{D}}(D) + \frac{qP_{\mathcal{E}}(E)}{(1-q)Q(E) + qP_{\mathcal{E}}(E)} Q(D). \quad (106)$$

One can show (Ref. [31], theorem 2.7.4) that the mutual information is convex in the second argument, that is, for a fixed marginal  $P(E)$ ,

$$\begin{aligned} I(D : E) [P(E), \lambda P^0(D|E) + (1-\lambda)P^1(D|E)] \\ \leq \lambda I(D : E) [P(E), P^0(D|E)] \\ + (1-\lambda)I(D : E) [P(E), P^1(D|E)]. \end{aligned} \quad (107)$$

In order to apply this fact to our problem, suppose that we fix the marginal  $P(E)$  – and consequently the fractions in the expression for  $P(D|E)$  above – but take a convex combination

$$P_{\mathcal{D}}(D) = \lambda P_{\mathcal{D}}^0(D) + (1-\lambda)P_{\mathcal{D}}^1(D), \quad (108)$$

so that the resulting  $P(D|E)$  is a convex combination with weight  $\lambda$  as well. In this case, an upper bound on the mutual information follows. It follows that, for fixed  $P_{\mathcal{E}}(E)$  and  $q$ , the largest mutual information is achieved when the distribution  $P_{\mathcal{D}}(D)$  is extremal, meaning that it produces one value with certainty. We express this as  $P_{\mathcal{D}}(D) = \delta(D)$  for short. We do not specify which value of  $D$  is found with certainty, since the mutual information depends only on the probabilities of different values, but not on their labels. By symmetry, in order to maximize the mutual information we must also have  $P_{\mathcal{E}}(E) = \delta(E)$ .

The maximal mutual information between  $D$  and  $E$  for a distribution constrained to the form (104) is therefore achieved by a distribution of the form

$$P(DE) = (1-q)Q(E)\delta(D) + qQ(D)\delta(E). \quad (109)$$

In order to evaluate the maximal mutual information explicitly, we make two simplifying assumptions: first, let us assume that the prior distributions  $Q(D)$  and  $Q(E)$  are both uniform, that is, that we have no additional information about them beyond what we can retrodict from  $B$ . Let us furthermore assume that  $D$  and  $E$  range over an equal number of values,  $N$ . Symmetry then suggests that the mutual information is maximal when  $q = \frac{1}{2}$ , which can be verified analytically. In this case, we obtain

$$I(D : E) = \log N - \frac{N+1}{N} [\log(N+1) - 1] \quad (110)$$

with  $\log$  denoting the logarithm used to calculate the entropy. By contrast, the maximal mutual information between  $D$  and  $E$  without any constraints is  $\log N$ . If  $D$  and  $E$  are bits ( $N=2$ ) and we calculate the logarithms in base 2, the upper bound on the mutual information becomes

$$I(D : E) \leq \frac{5}{2} - \frac{3}{2} \log_2(3) \approx .12. \quad (111)$$

Now consider the case where  $D$  and  $E$  are quantum systems. Their state under post-selection on a measurement outcome  $b$  on  $B$  can be written

$$\rho_{DE}^b = (1-q)\rho_D \otimes \frac{\mathbb{1}_E}{2} + q\frac{\mathbb{1}_D}{2} \otimes \rho_E. \quad (112)$$

As in the classical case, we consider the prior over  $D$  and  $E$  to be uniform, that is, the maximally mixed quantum state. This implies that there is in fact only one non-trivial density operator on  $D$  (in the first term) and  $E$  (in the second) in the entire problem. Consequently there exist preferred bases of  $\mathcal{H}_D$  and  $\mathcal{H}_E$ , namely the eigenbases of  $\rho_D$  and  $\rho_E$ , in which all density operators of interest are diagonal and thus effectively reduced to classical probability distributions. Therefore the results from the classical case carry over, and we recover the upper bound above as a function of the dimension of the Hilbert spaces  $N = \dim \mathcal{H}_D = \dim \mathcal{H}_E$ .

## SUPPLEMENTARY DISCUSSION

### Supplementary Discussion 1: Related work on superpositions of causal orders

We here discuss related work that considers the question of whether one can prepare a quantum-coherent mixture of different causal orders [14, 17]. For a pair of quantum systems,  $A$  and  $B$ , the idea is to prepare a quantum-coherent mixture of  $A$  being the cause of  $B$  and of  $B$  being the cause of  $A$ . By contrast, in this article we seek only to prepare a quantum-coherent mixture of  $A$  being a cause of  $B$  and of  $A$  and  $B$  having a common cause. There is an important difference between

the two objectives. In our case,  $A$  and  $B$  can be time-like separated, with  $A$  to the past of  $B$ . In the case of a quantum-coherent mixture of causal orders, on the other hand, the temporal order is different in the two terms of the mixture and consequently these must be embedded differently in space-time. This is the sense in which achieving a quantum-coherent mixture of causal orders requires one to abandon the assumption of a pre-defined global causal structure.

Nonetheless, the approach of defining probabilistic, physical, and quantum-coherent mixtures of causal relations that is espoused in the present article can be applied to the case of two cause-effect relations, in particular,  $A$  causing  $B$  and  $B$  causing  $A$ , and it is interesting to see what lessons are learned from doing so. We begin with the classical case.

In our approach, the overall causal structure of a given scenario is depicted by a directed acyclic graph (DAG). If one considers a probabilistic mixture of causal relations, then one must include enough causal influences in the graph to accommodate the causal relations that hold in any given element of the mixture. The DAG associated to a probabilistic mixture of cause-effect and common-cause, depicted in 8(b), therefore includes both a cause-effect pathway and a common-cause pathway between  $A$  and  $B$ . Similarly, it follows that the graph associated to a probabilistic mixture of  $A$  causing  $B$  and  $B$  causing  $A$  must have both a pathway wherein  $A$  causes  $B$  and another wherein  $B$  causes  $A$ .

Furthermore, as noted previously, in order to physically realize a probabilistic mixture of different causal relations, one requires a switch variable  $J$  that can influence one or more variables in the system and modify how they causally depend on other variables. For a probabilistic mixture of cause-effect and common-cause relations, it was shown in Supplementary Note 1 that this switch variable must influence  $B$  alone. But what does it imply for a probabilistic mixture of  $A$  causing  $B$  and  $B$  causing  $A$ ? In this case, the switch variable (call it  $J$ ) cannot influence  $B$  alone, but must instead influence both  $A$  and  $B$ . This is because as one varies between  $J = 0$  and  $J = 1$ ,  $A$  must toggle between having a causal dependence on  $B$  and not having such a dependence while  $B$  must simultaneously toggle between not having a causal dependence on  $A$  and having such a dependence. As such, the switch variable defines a common-cause pathway between  $A$  and  $B$ . The overall causal structure is depicted in 10.

One can immediately observe two uncomfortable facts about the overall causal structure.

First, the natural constraint on physical realizability of probabilistic mixtures articulated in Supplementary Note 1 has been violated. The objective was to have a probabilistic mixture of causal relations between  $A$  and  $B$  every element of which was purely cause-effect (either

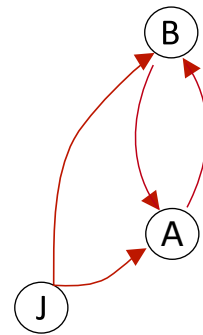


FIG. 10. **Mixture of causal orders** In order to physically realize a probabilistic mixture of different causal orders, one requires a switch variable  $J$  that can influence both variables  $A$  and  $B$ . One also requires a cycle in the causal structure.

$A$  causing  $B$  or  $B$  causing  $A$ ). However, any attempt to physically realize such a mixture introduces a causal relation that is not purely cause-effect, namely, the common cause  $J$ .

Second, and more importantly, one notes that the overall causal structure is not a directed acyclic graph because it includes a cycle. It is unclear how to make sense of such graph. One can no longer interpret the causal relations therein using the interventionist notion of causation that is standard for directed acyclic graphs. The reason is as follows. The interventionist notion of causation presumes that causal mechanisms in the graph are autonomous: the mechanism that describes how one variable in the graph is causally influenced by its parents can be varied independently of the mechanism that describes how any other variable in the graph is causally influenced by its parents. But this assumption of autonomy cannot be maintained in graphs with cycles. For instance, consider a graph having a cycle between a pair of binary variables,  $A$  and  $B$ . If the two causal mechanisms were autonomous, then it ought to be possible to take them to be  $A := B$  and  $B := A \oplus 1$  respectively. But the latter pair of mechanisms yields a contradiction, so the mechanisms cannot be varied independently of one another.

The second of these concerns may be surmountable in the case of a probabilistic mixture of  $A$  causing  $B$  and of  $B$  causing  $A$ , since only one of the two pathways is active for a given value of the switch variable  $J$ .

If, however, one considers instead a physical mixture of  $A$  causing  $B$  and of  $B$  causing  $A$ , then both pathways must be active simultaneously, and there is no way to deny the necessity of the cycle.

The conceptual problems introduced by the presence of cycles in the causal graph persist if one replaces classical variables with quantum systems. In the approach we propose in this article, a quantum-coherent mixture of causal relations between quantum systems is necessarily a physical mixture of those causal relations. Consequently, a quantum-coherent mixture of causal orders in



our approach requires a graph with a cycle, with all the interpretive ambiguity that this entails.

Finally, even if one can make sense of graphs with cycles, it remains unclear how one could ever hope to realize these experimentally because in the context of relativity theory, a causal cycle is a closed time-like curve which one expects is only physically realizable in very exotic physical scenarios. In our approach, therefore, realizing a quantum-coherent mixture of causal orders, if it is possible at all, is likely to only be possible in very exotic scenarios.

Some recent work by Procopio *et al.* [20] claims to achieve an experimental realization of a superposition of causal orders in a tabletop quantum optics experiment. This seems to contradict our claim that one is likely to require exotic physics to achieve such a thing. We therefore turn to the details of this experiment and why we do not believe that it can be accurately described as achieving a superposition of causal orders.

The objective is to realize, in a quantum optical setting, the quantum switch proposed by Chiribella *et al.* [32] and explored in Ref. [17], wherein the order of two gates is controlled by an ancillary quantum system that is prepared and post-selected in a superposition of the states which prescribe a definite causal order. This has been proposed as a means of achieving a superpo-

sition of causal orders. The experiment is based on a folded Mach-Zehnder interferometer whereby the order of two gates, call them  $U$  and  $V$ , is determined by the path taken by the photon. Due to the particular geometry, one requires a version of the  $U$  and  $V$  gate in each path of the interferometer.

This set-up is optically equivalent to an unfolded interferometer. In the latter case, it is clear that one requires a version of the  $U$  and  $V$  gate in each path of the interferometer, call them  $U_1, V_1$  and  $U_2, V_2$  respectively. The different orders that one switches between are:  $U_1$  is implemented and then  $V_2$  is implemented, and  $U_2$  is implemented and then  $V_1$  is implemented. The situation is clearly not one wherein one toggles between a photon passing through two fixed spatio-temporal regions in one of two different orders.

For the case of the folded interferometer used in the experiment, it is still the case that one requires two versions of each gate; it is simply that the two versions correspond to the gate functioning at different times. Call the early versions of the two gates  $U_1, V_1$  and the late versions  $U_2, V_2$ . Again, the different orders that one switches between are:  $U_1$  is implemented and then  $V_2$  is implemented, and  $U_2$  is implemented and then  $V_1$  is implemented.

If one instead required that each gate act only once in a localized spatio-temporal region – for instance, by putting shutters that let a photon through the gate only in a narrow window of time – then the experimental set-up in question would no longer realize a quantum switch.